ATG2A engages Rab1a and ARFGAP1 positive membranes during autophagosome biogenesis

Devin M. Fuller[1,2], Yumei Wu[1-5#], Florian Schueder[1,6#], Burha Rasool[1], Shanta Nag[1], Justin L. Korfhage[1], Rolando Garcia-Milian[7], Katerina D. Melnyk[1], Joerg Bewersdorf[1,8,9,10,11], Pietro De Camilli[1-5], Thomas J. Melia*[1,2]

[1] Department of Cell Biology, Yale University School of Medicine, New Haven, CT
[2] Aligning Science Across Parkinson's (ASAP) Collaborative Research Network, Chevy Chase, 20 MD
[3] Department of Neuroscience, Yale University School of Medicine, New Haven CT
[4] Howard Hughes Medical Institute, Yale University School of Medicine, New Haven, CT
[5] Program in Cellular Neuroscience Neurodegeneration and Repair, Yale University School of Medicine, New Haven, CT
[6] Department of Microbial Pathogenesis, Yale School of Medicine, New Haven, CT, USA
[7] Bioinformatics Support Hub, Yale Medical Library, Yale School of Medicine, 333 Cedar St, New Haven, CT 06510
[8] Department of Biomedical Engineering, Yale University, New Haven, CT, USA
[9] Nanobiology Institute, Yale University, West Haven, CT, USA
[10] Kavli Institute for Neuroscience, Yale School of Medicine, New Haven, CT, USA
[11] Department of Physics, Yale University, New Haven, CT, USA
[#] these authors contributed equally

*Corresponding author: Thomas Melia

Email: Thomas.melia@yale.edu

Author Contributions: TJM and DMF conceptualized the project. FS and JB designed and performed the FLASH-PAINT analysis. YW and PDC designed and performed the correlative light electron microscopy experiments. DMF performed all other experiments reported in this study with contributions from BR, SN, JLK, RGM and KDM The manuscript was prepared by DMF and TJM with input from all authors.

Competing Interest Statement: FS and JB filed patent applications with the U.S. patent office covering FLASH-PAINT. JB has licensed IP to Bruker Corp. and Hamamatsu Photonics. JB is a founder of panluminate, Inc.

Abstract

Autophagosomes form from seed membranes that expand through bulk-lipid transport via the bridge-like lipid transporter ATG2. The origins of the seed membranes and their relationship to the lipid transport machinery are poorly understood. Using proximity labeling and a variety of fluorescence microscopy techniques, we show that ATG2A localizes to extra-Golgi ARFGAP1 puncta during autophagosome biogenesis. ARFGAP1 itself is dispensable during macroautophagy, but among other proteins associating to these membranes, we find that Rab1 is essential. ATG2A co-immunoprecipitates strongly with Rab1a, and siRNA-mediated depletion of Rab1 blocks autophagy downstream of LC3B lipidation, similar to ATG2A depletion. Further, when either autophagosome formation or the early secretory pathway is perturbed, ARFGAP1 and Rab1a accumulate at ectopic locations with autophagic machinery. Our results suggest that

ATG2A engages a Rab1a complex on select early secretory membranes at an early stage in autophagosome biogenesis.

Significance Statement

This study elucidates the role of early secretory membranes in autophagosome biogenesis. The authors demonstrate that Rab1/ARFGAP1 positive membranes are essential to autophagy and are recruited to the phagophore assembly site at an early step of autophagosome biogenesis. These membranes interact with the bridge-like lipid transport protein ATG2A and are positive for LC3B and WIPI2, suggesting that Rab1 membranes are a direct source for autophagosome growth.

Main Text

Introduction

Macroautophagy is a cellular degradative pathway in which a seed vesicle grows to encapsulate a target cargo, closes to form the complete autophagosome, and subsequently fuses with the lysosome. This transient organelle forms *de novo* in approximately ten minutes and requires the delivery of millions of lipids[1]. ATG2 proteins function as bridge-like bulk lipid transport proteins[2-5] and are essential during the membrane expansion step of autophagosome biogenesis. We propose that ATG2 bridges the ER and the developing phagophore, thereby allowing lipids to cross the cytosol through a long hydrophobic groove[3]. At the phagophore, lipids are equilibrated into both leaflets of the bilayer via the ATG9 scramblases[6-8]. As such, ATG9 is essential to macroautophagy and is a key component of the seed membranes that ultimately expand during ATG2-mediated lipid transport[9, 10].

In addition to ATG9 vesicles, several other membrane sources have been proposed to be involved in autophagosome biogenesis. In particular, both genetics and biochemistry implicate an essential role for the early secretory pathway. In yeast, some COP-II vesicle and ER exit site (ERES) proteins contribute to starvation-mediated autophagy at a stage that is downstream of formation of the pre-autophagosome structure (PAS)[11, 12]. Furthermore, yeast ERES naturally colocalize with the autophagic cargo Ape1[13], and that colocalization increases when various autophagy factors are depleted[13, 14]. These studies imply that autophagosome initiation events may not be dependent upon the secretory pathway, but subsequent membrane growth or autophagosome maturation requires active ERES structures. Cross linking studies further establish a close proximity between autophagy and ERES proteins[15]. Finally, the direct integration of yeast COPII-derived membranes into developing phagophores is suggested by the detection of the COP-II cargo Axl2-GFP, a transmembrane protein, at both phagophores and mature autophagosomes[16].

In human cell lines, genetic or pharmacological disruption of the COPII-related small GTPase Sar1a reduces the frequency of autophagic events[17]. Following biochemical fractionation of cellular membranes, the ER-to-Golgi Intermediate Compartment (ERGIC) is especially competent for supporting in vitro lipidation by LC3B, the primary marker of autophagic structures[17, 18] and clusters of COPII positive membranes can be seen accumulating adjacent to phagophores[19]. Like in yeast, these studies can be interpreted as a key role for ERES or ERGIC membranes in forming or expanding autophagosome membranes. As starvation-mediated macroautophagy drives substantial remodeling of both the ERES and ERGIC membranes (Liang Ge review;), including the formation of subdomains with unique protein-dependent organelle-organelle contact sites[20], it is possible that the ERES/ERGIC contribution to autophagy represents a distinct subcompartment of these membrane structures.

Presumably, any contribution of an early secretory membrane must ultimately coordinate with recruitment of ATG9 vesicles, in order to ensure that the lipid transport machinery is competent to expand the phagophore membrane. Several studies have postulated an early fusion intermediate in phagophore formation, such as the description of the HyPas compartment where vesicles bearing distinct autophagy proteins (ATG16L1 and FIP200) were observed to coalesce early in autophagosome biogenesis[21]. Intriguingly, when the lipid transporter ATG2 is genetically depleted from cells, all of the essential autophagy machinery including ATG9 concentrates into large compartments[9, 22-24]. Correlative light and electron microscopy of these structures indicate they are large assemblies of ATG9 vesicles surrounded by more complex membranes which harbor FIP200 and WIPI2, among other proteins[9, 25]. These complex membranes often adopt a cup-like shape, leading us to name them “proto-phagophores”[9]. The origins of the proto-phagophores have been unknown.

In this study, we demonstrate that ATG2A is enriched during autophagosome biogenesis at Rab1/ARFGAP1 positive membranes. Although both proteins can be found within the ERGIC compartment, proximity data and colocalization analyses in secretory pathway disrupted cells suggest that Rab1 and ARFGAP1 membranes involved in ATG2 recruitment are distinct from generic ERGIC membranes. Genetic depletion experiments indicate that Rab1 and ATG2 function at a similar step in autophagosome formation and further these proteins can be isolated together in a complex. Finally, both ARFGAP1 and Rab1 co-localize with proto-phagophores, implying these membranes can recruit much of the key early autophagy machinery and may be dynamically remodeled into cup-like morphologies.

Results

ATG2A is proximal to early secretory membranes

To determine the local proteome adjacent to ATG2A, we used a proximity labeling approach. We fused the biotinylation enzyme APEX2 and a green fluorescent marker to the amino-terminus of ATG2A (APEX2-EGFP-ATG2A) and expressed this construct in ATG2A/B double knockout cells (ATG2 DKO cells). In this way, the APEX2 enzyme will biotinylate cellular proteins in close proximity to the expressed ATG2A fusion protein[26]. To ensure that the APEX2-EGFP-ATG2A construct is active and correctly localized, we measured the restoration of macroautophagy in these cells by following LC3B flux and p62 clearance (Fig. S1 A-C). While both LC3B-II and p62 dramatically accumulate in the ATG2 DKO cells, this accumulation is almost entirely reversed upon re-expression of APEX2-EGFP-ATG2A.

We also validated that biotinylation in these cells depends upon the presence of APEX-EGFP-ATG2A and a full reaction. In cells expressing APEX2-EGFP-ATG2A, biotin is only observed when both the biotin substrate (biotin phenol) and the reaction promoter (hydrogen peroxide) are included (Fig. S1 D and E). Likewise, streptavidin-mediated immunoprecipitation revealed a strong enrichment of biotinylated material only when the full reaction conditions were employed (Fig. S1F). Furthermore, the anti-biotin and GFP signals colocalized establishing that biotinylation is favored at sites proximal to ATG2A (Fig. S1D).

Mass spectrometry of proteins isolated by streptavidin-mediated immunoprecipitation was performed using a three state quantitative SILAC experiment[26] with light, medium, and heavy isotopes as follows: no hydrogen peroxide as a negative control, a full reaction in complete media, and a full reaction in starvation media and 100 nM bafilomycin. When comparing both the heavy and medium isotope states to the light state, mass spectrometry analysis revealed an abundance of autophagy related proteins in both full media and under starvation (Figs. 1A and S1G, respectively). The majority of these proteins were cargo adaptors such as NBR1, p62 (SQSTM1), and TAX1BP1, suggesting that the target cargo is immediately adjacent to the biogenesis machinery during autophagosome maturation. We also observed a clear enrichment

of ERES or COPII proteins including Sec16A, Sec23A, Sec23IP, and Sec24B/C. Additional ERES proteins such as TFG and Sec31A were also enriched in some, but not all, of the three replicates. In addition, ARFGAP1, a COPI effector that is primarily localized to the Golgi but also found in earlier secretory membranes, was one of the two most enriched proteins in both full media and starvation. Both ARFGAP1 and the COPII proteins suggest ATG2 is localizing to the early secretory pathway.

ATG2A is recruited to ARFGAP1 membranes during autophagosome biogenesis

As an orthogonal method to assess the proximity of ATG2A to early secretory components, we performed FLASH-PAINT, a super resolution technique with high multiplexing capabilities[27]. FLASH-PAINT offers sub-organelle resolution while simultaneously allowing us to screen >10 proteins. ATG2 DKO cells stably expressing GFP-ATG2A were starved and then immunostained for autophagic proteins (GFP-ATG2A, p62, and LC3B), ERES proteins (Tango1, Sec24C, Sec31A, Sec16A, TFG), and markers of COPI-positive membranes (ARFGAP1 and COPI). All proteins were concurrently labeled with primary antibodies that were in turn identified by their association with secondary antibodies with unique DNA barcodes (Fig. S1I). A fluorophore conjugated imager DNA strand and adaptor strands were added to target the imager to the correct secondary antibody. Eraser strands were added in between rounds of imaging to outcompete the adaptor and allow for sequential labeling. In this way, the sub-cellular localization of all ten proteins could be established within the same image.

In these images, the Golgi can easily be identified as a perinuclear ribbon staining strongly for both ARFGAP1 and COP1 (magenta and purple respectively, Fig. S1J). In addition, there are bright puncta throughout the cell (pink arrow heads) stained with TFG and Sec31A, indicating that they are ERES. ARFGAP1 and COPI frequently also accumulated at ERES (made more obvious in the top-right inset, where TFG and Sec31 are removed), consistent with previous reports that COPI vesicles facilitate ER to Golgi transport in human cells[28-30]. GFP-ATG2A is mostly cytosolic, however small accumulations of ATG2 could be found at ERES and were generally observed to be proximal to ARFGAP1/COP1 (inset; brackets). Note that clusters of LC3B and p62 are also present. Occasionally, non-ERES accumulations of p62 could be observed in close proximity to LC3B and ATG2A (lower insets), and here again ATG2 is proximal to ARFGAP1.

Critically, we can directly measure the nominal proximity of each protein relative to the others under investigation by quantifying the median distance between all ten tested proteins within 200 nm of each individual protein (Fig. S1K). All early secretory pathway proteins closely associate with each other, including the COPI proteins ARFGAP1 and β-COP. As the majority of ATG2A was cytosolic, its average distances from other proteins were greater, however, within this cohort of candidate proteins, we found that ATG2A is most closely associated with P62 and ARFGAP1 (15nm and 16nm respectively; top row of Fig. S1J), exactly consistent with the APEX screen.

The APEX and FLASH-PAINT datasets provided a clear but static result that ATG2A is recruited to ARFGAP1 positive structures. To determine whether this recruitment was coincident with phagophore formation, we stably expressed GFP-ATG2A and TagBFP-LC3B in ATG2 DKO cells in order to identify phagophores. ATG2A primarily localizes to phagophores and lipid droplets, whereas LC3B primarily localizes to phagophores, autophagosomes and autolysosomes. Where these two proteins colocalize strongly suggests a growing phagophore in the process of membrane expansion (Figs. 1B). To assess co-localization with phagophores, we expressed candidate early secretory proteins labeled with red fluorophores (Fig. 1 C and D**)**. ARFGAP1-TagRFP colocalized with ~90% of actively forming phagophores, whereas only ~30% of phagophores were coincident with the ERES markers mRuby-Sec23A or RFP-p125a/Sec23IP. Further, while the ARFGAP1 signal was largely concentrated in the Golgi, phagophores most frequently colocalized with extra-Golgi ARFGAP1 puncta.

Finally, we compare our results to the subcellular localization of ATG2 established by global organelle profiling available at the database at https://organelles.sf.czbiohub.org[31]. Both ATG2A and ATG2B are highly enriched at membranes isolated via Rab1a immunoprecipitation, but were not enriched in Sec23A, Sec31A, or COPI isolates (Fig. 1E). Also present were two known interactors of ATG2 proteins, the ATG9A lipid scramblase and the PI3P-binding adaptor WDR45/WIPI4. Likewise, ARFGAP1, but not ARFGAP2 or ARFGAP3, was also highly enriched at Rab1a membranes. These collective results establish that both endogenous ARFGAP1 (organelle isolation, APEX, FLASH PAINT) and overexpressed ARFGAP1 (live imaging) naturally associate with ATG2A, including during phagophore biogenesis.

Autophagic flux depends upon Rab1 but not ARFGAP1

To look for a potential functional role for ARFGAP1 in autophagy, we measured autophagic flux using the HaloTag dropout assay in which liberation of a free HaloTag (HT) is indicative of lysosome-mediated proteolysis of the full-length (FL) protein[32]. We stably expressed HaloTag7-mGFP-LC3B in WT HEK293 cells and then used siRNA to knockdown various regulators or potential regulators of macroautophagy initiation (Fig. 2 A and B). Despite efficient knockdown, siRNA against ARFGAP1 had very little effect on flux; the ratio of free HaloTag to full-length HaloTag7-mGFP-LC3B following ARFGAP1 knockdown was similar to both nontransfected (NT) and nontargeting siRNA controls. In contrast, knockdown of the autophagy initiation factor FIP200 dramatically suppressed dropout of the HaloTag. We also looked for an interaction between ARFGAP1 and ATG2A, but even when both proteins were overexpressed, we could not detect significant interaction via co-immunoprecipitation (Fig. 2 E and F). Thus, it is likely that ARFGAP1 localizes to a key membrane involved in autophagosome biogenesis but is not itself a player in initiating autophagosome formation.

As shown in (Fig. 1E), both the ATG2/ATG9 lipid transport apparatus as well as ARFGAP1 are associated to Rab1A-positive membranes. Rab1 proteins mediate ER to Golgi trafficking in the early secretory pathway. The yeast Rab1 homologue, Ypt1, is essential to autophagy[33, 34], while in mammals, genetic depletion of either Rab1a or Rab1b modestly reduces autophagic flux[35, 36]. Thus, we tested the functional and physical interaction of Rab1 proteins with ATG2. Consistent with previous results, siRNA knockdown of either Rab1a or Rab1b in our system partially inhibited flux in the Halo dropout assay (Fig. 2 A and B). Strikingly, knockdown of both homologues simultaneously was nearly as effective as knocking down FIP200, establishing that Rab1 proteins play an essential role in supporting starvation induced autophagic flux.

In addition to following the Halo-tagged LC3B, we also immunoblotted for endogenous LC3B in each of our siRNA experiments. We found that knockdown of either Rab1 isoform, and especially knockdown of both together leads to a clear accumulation of the membrane conjugated form of LC3B, LC3B-II (Fig. 2A). As LC3B overexpression can alter endogenous LC3B patterns, we confirmed this increase in a cell line expressing only HaloTag7-mGFP (Fig. 2 C and D). Knockdown of Rab1a and Rab1b drove a threefold increase of LC3B-II (Fig. 2D).

Increasing LC3B-II levels without autophagic flux is indicative of a block to macroautophagy at a late stage, downstream of initiation, and is therefore easily distinguished from the block induced by depleting FIP200 (where LC3B-II levels go down). Intriguingly, LC3B-II levels also increase when ATG2 proteins are genetically depleted (Fig. S1A,B), suggesting ATG2A and Rab1a might function together. Indeed, overexpressed GFP-Rab1a could strongly immunoprecipitate flag-tagged ATG2A in our cells, indicating these proteins are in a shared complex (Fig. 2 E and F).

We also tested several other proximity hits from the biotinylation analysis for interaction with flag-tagged ATG2A, including GFP-tagged copies of ERES resident proteins Sec23A, Sec31A, Sec16A, Sar1 and all four homologs of Sec24 (Fig. S2 A-D). We found that ATG2A co-immunoprecipitated weakly with many of them, the strongest of which was Sec24D. Note that this Sec24D interaction was barely above the background of pull-down with GFP alone (Fig. 2 E and

F). Thus, consistent with proximity and imaging analyses, ATG2 proteins are in the general proximity of the ERES machinery, but protein-protein interactions appear to be limited to Rab1.

Disruption of the early secretory pathway results in the recruitment of autophagic proteins to Rab1a-positive tubular membranes

These results suggest that ATG2 engages an early secretory membrane, distinct from the ERES, in a Rab1-dependent manner. We next tested whether disruption of the early secretory system would impact the localization of ATG2A. To this end, we overexpressed Sar1bH79G, the catalytic dead mutant of the small GTPase Sar1b that recruits the COPII coat. Sar1bH79G binds the membrane and recruits the COPII coat, but is unable to release, thereby trapping COPII onto the membrane. Overexpression of this construct has been shown to reduce autophagy in starved cells[17, 35]. Consistent with those results, overexpression of Sar1bH79G-mOrange2 diminished autophagic flux of both a bulk cargo (HaloTag7-mGFP reduced ~20%) and of LC3B (HaloTag7-mGFP-LC3B reduced by ~30%) by the HaloTag degradation assay[32] (Figs 3A/B). Further, LC3B puncta number were lowest in cells expressing high amounts of Sar1bH79G (Figs. S3A/B), consistent with a block to autophagosome formation rather than autophagosome clearance.

Unexpectedly, in a small subset of transfected cells (1.5±0.8%), overexpression of Sar1bH79G under starvation conditions shifted the localization of GFP-ATG2A from a largely punctate distribution to long, tubular objects that were Sar1bH79G negative (Fig 3C). GFP-ATG2A decorated these tubules with varying intensities approximating a beads-on-a-string pattern (e.g. arrows in Fig. 3 D and E). Fluorescently tagged forms of LC3B, ARFGAP1 and Rab1a also decorated these tubules. However, these three proteins displayed the brightest intensities where ATG2A was dimmer (e.g. arrowheads in Fig. 3 D and E). These three proteins, but not ATG2A, also decorated larger structures that appeared to be contiguous with the tubule, including bulbous regions at the tubule termini.

To determine the ultrastructure of these regions, we subjected GFP-ATG2A-expressing cells to correlative light and focused ion beam scanning electron microscopy (CLEM-FIB-SEM). The GFP-ATG2A fluorescence signal corresponded to thin, tubular membranes (Fig. 3F and S3C), which is consistent with the finding that ATG2A preferentially binds highly curved membranes[37]. The tubule is surrounded by ER elements, many of which appear to be in very close contact (Fig. 3F, S3C). GFP-ATG2A signal was more intense in regions with closely adjacent ER, consistent with a possible contact site localization. The tubule continued into larger structures at either end, which were GFP-ATG2-negative, and morphologically similar with the bulbous structures harboring ARFGAP1, Rab1a and LC3B in fluorescence images.

Thus, although unusual, these rare tubules afforded an opportunity to demonstrate that ATG2, ARFGAP1 and Rab1a target the same membrane, easily resolvable even at confocal resolution. ATG2 collects where ER is closely adjacent, and LC3B accumulates with Rab1a, implying a topological organization with LC3B and Rab1a decorating the same structure, suggesting that Rab1a membranes may be a component or progenitor of the phagophore membrane.

ARFGAP1 and Rab1a accumulate around pre-autophagic structures in ATG2 DKO cells

We previously published that very small, ATG9- and LC3B-positive vesicles accumulate in large clusters with the cargo-adaptor p62 in ATG2 DKO cells[9]. This cluster is surrounded by a shell of more complicated membranes which we termed “protophagophores” because they colocalize with other autophagy proteins such as WIPI2 and because many of them appear to adopt a cup-like shape in TEM images. Beyond this protophagophore shell, the entire structure is surrounded by ER (illustrated in Fig. 4A). Our work and others have shown that essentially all proteins involved in autophagosome biogenesis accumulate with these clusters, including FIP200, ATG14, ATG9A, ATG16L, and p62[9, 22, 23], suggesting they are repositories of autophagosome biogenesis

material awaiting the arrival of ATG2 proteins. If early secretory membranes contribute directly in any way to the biogenesis event, they may also concentrate at these sites.

We therefore performed IF against various markers of the early secretory pathway in ATG2 DKO cells to look for colocalization with this compartment (represented by staining for p62 (mouse antibody) or for LC3B (rabbit antibody); Figs. 4B-D). We found that ER exit site markers such as Sec16A, Sec24C, Sec31A, and TFG were not enriched around the compartment, neither was the Golgi protein GM130 (Figs. 4C-D and S4A). ßCOP was modestly enriched, but at levels that by eye, did not suggest encapsulation of the compartment the way autophagy proteins collect. In addition, overexpressed mEmerald-ERGIC53 did not localize to the ATG2 DKO compartment (Fig. S4B). In contrast, ARFGAP1 targeted essentially all of the ATG2 DKO compartments, forming a robust spherical shell at the periphery of the p62 signal (Fig. 4B-D). This distribution was maintained during mitosis in contrast to the ARFGAP1 signal in the Golgi, which dissipated (Fig. 4B).

We were unable to find a strong Rab1a signal by immunofluorescence, however, when overexpressed, GFP-Rab1a also formed a sphere around the ATG2 DKO compartment (Fig. 4E). Both ARFGAP1 and SNAP-Rab1a colocalized with WIPI2 (Fig. 4F), consistent with a model whereby these membranes arrive at the PAS prior to ATG2A recruitment and subsequent autophagosome biogenesis.

Discussion

Here we describe an interaction of ARFGAP1/Rab1-positive membranes with the autophagic biogenesis machinery including the lipid transporter ATG2. These membranes likely derive from a privileged region of the ERGIC consistent with the literature tying these intermediate secretory membranes to autophagy[17, 20]. In particular, the presence of both ARFGAP1 and Rab1 plus the general proximity to ERES proteins across a variety of assays is consistent with an early secretory origin for these membranes. Intriguingly, ARFGAP1 and Rab1 coalesce around the periphery of the ATG2 DKO compartment exactly where we previously described complex cup-shaped membranes, so called proto-phagophores[9], accumulate. We do not detect any other ERES or ERGIC markers at these sites, implying proto-phagophores derive from only a subdomain of the ERGIC which we suspect is remodeled specifically for the purpose of supporting autophagy.

What do the ERGIC-derived membranes contribute to autophagosome formation? We speculate on three possibilities: 1) Local proteins are needed to drive other early autophagy steps. Most notably, in addition to interacting with ATG2A as shown here, Rab1 proteins also interact with other early acting autophagy proteins[33, 34, 38] including especially the PI3Kinase, VPS34[39, 40]. Thus, a privileged region of the ERGIC may simply best coordinate the machinery driving local protein and lipid remodeling needed to initiate phagophore formation. 2) ERGIC-derived membranes may have a unique membrane composition and structure necessary for autophagosome biogenesis. The Rab1-positive membranes that accumulate around the core of ATG9 vesicles in the DKO compartment are enriched for cup-like morphologies[9]. We do not yet know the structural basis for these morphologies, but it may be that membranes with a natural degree of plasticity, as has been shown for the complex network of structures emanating from COPI/COPII rich early secretory membranes[28], are better adapted to the subsequent remodeling needed to shape and grow around cytoplasm isolates during starvation-mediated macroautophagy. 3) Small ATG9 vesicles may not contribute sufficient volume to grow a phagophore, even considering the very small luminal volume of a mature autophagosome. Geometric estimates of the surface-to-volume ratio in yeast autophagosomes, gleaned from cryo-electron microscopy tomograms, suggest that as much as 20% of the membrane might derive from fusion rather than lipid transport in order to deliver volume[41]. Autophagosome biogenesis also depends upon the incorporation of ATG9 scramblases[42], which are thought to be delivered

from a trans-Golgi compartment to the site of autophagosome biogenesis. As both the ERGIC and ATG9 seed membranes collect to high local concentrations in ATG2 DKO cells, future work may be able to tease out how their separation and eventual coalescence are regulated.

Materials and Methods

Plasmids and reagents

The following plasmids were used in this study: pLVX Puro GFP-ATG2A (Previously published[3]), pLVX Puro APEX2-GFP-ATG2A (This study; a PCR fragment containing flanking EcoRI cutsites around APEX2 was generated from pcDNA3 APEX2-NES (Addgene #49386) and was inserted into GFP-ATG2A by ligation), pCMV 3xFLAG-ATG2A (Previously published[3]), pLVX Neo TagBFP-LC3B (This study; pLVX puro TagBFP-LC3B[3] and pLVX-EGFP-IRES-Neo (Addgene #128660) were cut with EcoRI and BamHI, following which the TagBFP-LC3B fragment was ligated into the pLVX Neo backbone), pDESt47 Sar1-GFP (Addgene #67409), Sar1b-mOrange2 (Addgene #166899), Sar1bH79G2-mOrange2 (Addgene #166900), Sar1bH79G-3xFLAG (This Study; A BamHI-3xFLAG-NotI fragment was generated by oligo annealing, following which it was ligated into the Sar1bH79G-mOrange2 backbone that was cut by the same restriction enzymes), mRuby-Sec23A (Addgene 36158), EGFP-Sec23A (Addgene #66609), pEGFP-Sec24A (This Study; a XhoI-Sec24A-PacI fragment was generated by PCR from HA-Sec24A which was a generous gift from the Kundu lab. The fragment was ligated into the backbone of pEGFP-Sec24D, which was cut by the same restriction enzymes), pEGFP-Sec24B (This Study; a XhoI-Sec24B-PacI fragment was generated by PCR from HA-Sec24B which was a generous gift from the Kundu lab. The fragment was ligated into the backbone of pEGFP-Sec24D, which was cut by the same restriction enzymes), EGFP-Sec24C (This Study; a AgeI-EGFP-XhoI fragment was generated by PCR and was ligated into the backbone of pEYFP-Sec24C (Addgene #66608) which was cut by the same restriction enzymes), pEGFP-Sec24D (Addgene #32678), GFP-Sec31A (Addgene #42124), GFP-Sec16A (Addgene #36155), ARFGAP1-TagRFP (This Study; ARFGAP1-TagRFP was a gift from the Rothman lab. A frame shift and a point mutation were corrected by site directed mutagenesis), ARFGAP1-GFP (Gift from the Antonny Lab), pMRX IB HaloTag7-mGFP (Addgene # 184903), pMRX No HaloTag7-mGFP-LC3B (Addgene # 184901), pLVX GFP (This Study; a fragment containing EGFP was generated from pLVX GFP-ATG2A and was ligated into pLVX puro (Clonetech, 632159) that was cut with EcoRI using Gibson Assembly), GFP-Rab1a (Gift from the Rothman Lab), SNAP-Rab1a (Gift from the Rothman Lab)

Antibodies for immunoblotting were used at 1:1000 and include the following: anti-ATG2A (Cell Signaling Technology, 15011S), anti-P62 (BD BioSciences, 610832), anti-GAPDH (Abcam, ab9484), anti-LC3B (Cell Signaling Technology, 3868S), anti-RB1CC1 (Thermo Fisher Scientific, 172501AP), anti-Rab1a (Cell Signaling Technology, D3X9S), anti-Rab1b (Proteintech, 17824-1-AP), anti-ARFGAP1 (Proteintech, 13571-1-AP), anti-FLAG (Sigma-Aldrich, F1804-200UG), anti-GFP (Cell Signaling Technology, 2956S), anti-mCherry (Invitrogen, PA5-34974), ECL anti-rabbit IgG horseradish peroxidase-linked (GE Healthcare, NA934V), and ECL anti-mouse IgG horseradish peroxidase-linked (GE Healthcare, NA931V).

Antibodies for immunofluorescence were used at 1:500 and include the following: anti-Biotin (Rockland, 200-301098S), anti-GFP nanobody (Massive Photonics), anti-ARFGAP1 (Proteintech, 13571-1-AP;), anti-Sec31A (BD Biosciences, 611280), anti-Sec24C (Cell Signaling Technology, 14676S), anti-MIA3 (Tango1; Sigma, HPA055922), anti-TFG (Abcam, ab156866), anti-COPI (CMIA10; made by Rothman Lab), anti-LC3B (MBL, PM036), anti-P62 (BD BioSciences, 610832), anti-Sec16A (Abcam, ab70722), anti-Sec24D (Cell Signaling Technology, 14687S), anti-GM130 (Proteintech, 11308-1-AP), anti-ERGIC53 (Abcam, EPR6979), Alexa Fluor 405 goat anti-rabbit IgG (Thermo Fisher Scientific, A31556), Alexa Fluor 405 goat anti-mouse IgG (Thermo Fisher Scientific, A31553), Alexa Fluor 594 goat anti-rabbit IgG (Thermo Fisher Scientific,

A11037), Alexa Fluor 647 goat anti-rabbit IgG (Thermo Fisher Scientific, A21245), and Alexa Fluor 647 goat anti-mouse IgG (Thermo Fisher Scientific, A21236).

The following reagents were purchased for FLASH-PAINT: Cy3B-modified DNA oligonucleotides were custom-ordered from IDT. Sodium chloride 5 M (cat: AM9759) were obtained from Ambion. Ultrapure water (cat: 10977-015) was purchased from Invitrogen. µ-Slide 8-well chambers (cat: 80807) were purchased from ibidi. Methanol (cat: 9070-05) was purchased from J.T. Baker. Glycerol (cat: 65516-500ml), protocatechuate 3,4-dioxygenase pseudomonas (PCD) (cat: P8279), 3,4-dihydroxybenzoic acid (PCA) (cat: 37580-25G-F) and (+−)-6-hydroxy-2,5,7,8- tetramethylchromane-2-carboxylic acid (Trolox) (cat: 238813-5 G) were ordered from Sigma. 1× Phosphate Buffered Saline (PBS) pH 7.2 (cat: 10010-023) was purchased from Gibco. Paraformaldehyde (cat: 15710) were obtained from Electron Microscopy Sciences. Bovine serum albumin (cat: 001-000-162) was ordered from Jackson ImmunoResearch. Triton X-100 (cat: T8787-50ML) was purchased from Sigma-Aldrich. DNA labeled Nanobodies were obtained from Massive Photonics.

SiControl, FIP200, Rab1a, Rab1b, and ARFGAP1 were acquired from Horizon Discovery (D-001810-10-05, L-0082383-00-0005, L-008958-01-0005, L-013321-02-005; Horizon Discovery).

Cell culture

HEK293 cells (ATCC, CRL-1573) were cultured at 37°C and 5% CO2 in DMEM (Thermo Fisher Scientific, 11965092) supplemented with 10% FBS (Thermo Fisher Scientific, 10438062) and 1% penicillinstreptomycin (Thermo Fisher Scientific, 15140122). Cells were starved by incubation in Earle's Balanced Salt Solution (Thermo Fisher Scientific, 24010043) for biochemical assays or in Hank's Balanced Salt Solution (Thermo Fisher Scientific, 14025092) for live cell imaging assays and treated with 0.1 µM bafilomycin A1 (Enzo, BML-CM110-0100) for 2 h.

Lentivirus production and transduction

HEK293 cells were seeded into a 10-cm plate. At 70% confluence, cells were transfected with 4.3 µg psPAX2 (Addgene #12260), 0.43 µg pCMV-VSV-G (Addgene, #8454), and 4.3 µg target plasmid using 20 µl Lipofectamine 3000 (Thermo Fisher Scientific, L3000008). DNA was added to 500 µl Opti-MEM (Thermo Fisher Scientific, 31985070) and Lipofectamine 3000 to 500 µl Opti-MEM in separate 1.5 ml microcentrifuge tubes. The tubes were then mixed and left for 10 min before adding the mixture dropwise to cells in fresh DMEM. After overnight incubation at 37°C, the medium was replaced with fresh DMEM. Cell medium was then collected after 24-48 h and filtered with a 0.45-µm syringe filter (Pall, 4184). Generated virus was either used immediately or was aliquoted and stored at −80°C. HEK293 cells to be transduced were seeded into a 6-well plate. Undiluted virus was added to cells and incubated at 37°C for 24 h. The medium was replaced with fresh DMEM and left for another 24 h. The cells were then treated with 2 µg/ml puromycin (Clontech, 631306), 2 mg/ml Geneticin (Thermo Fisher Scientific, 10131035), or 10 µg/ml Blasticidin (Gibco, A11139-03) for at least 2 wk. For the case of pMRX No HaloTag7-mGFP-LC3B, which lacked a selection marker, the cells were transduced and subsequently sorted by flow assisted cell sorting to normalize GFP expression levels.

Proximity labeling

Proximity labeling was performed as previously described[26]. ATG2 DKO cells stably expressing APEX2-EGFP-ATG2A were cultured for two weeks in media containing heavy, medium, or light isotopes of arginine and lysine (Cambridge Isotope Laboratories, CLM-2265-H-PK, DLM-2640-PK, CNLM-291-H-PK; Sigma-Aldrich, 608033). All conditions were expanded to 3x15cm plates prior to proximity labeling. Heavy labeled cells were starved in EBSS and treated with 100 nM Bafilomycin A1 (Enzo, BML-CM110-0100) for 2 hrs prior to labeling. All conditions were incubated with 500 µM Biotin Phenol (Biotinyl Tyramide; Sigma-Aldrich, SML2135) for 30 min at 37°C. The

heavy and medium isotope conditions were treated with 1 mM H2O2 (Sigma-Aldrich, H1009-100ML) for 1 min at room temperature. All conditions were then aspirated and scraped in quencher solution containing 10 mM sodium azide (Sigma-Aldrich, S2002-100G), 10 mM sodium ascorbate (Sigma-Aldrich, A4034-100G) and 5 mM Trolox (Sigma-Aldrich, 238813-5G) in DPBS. The cells were then spun down at 77xg for 5 min at 4°C and were resuspended in quencher solution. This process was repeated for a total of three washes. The cells were then lysed in RIPA buffer (50 mM Tris, 150 mM NaCl, 0.1% SDS, 0.5% sodium desoxycholate, 1% NP40 and 1x protease inhibitor (Roche)) for 30 min prior to centrifugation for 10 min at 18,407xg at 4°C. The supernatants were collected and protein concentration was assessed via bradford assay. Heavy, medium and light cells were mixed at a 1:1:1 ratio for a combined mass of 3-4 mg of protein. The protein mixtures were subsequently incubated with streptavidin magnetic beads (Pierce, 88817) for 2 hrs at 4°C after which they were washed twice with RIPA lysis buffer, once with 1 M KCl, once with 0.1 M Na_2CO_3, once with 2 M urea in 10 mM Tris-HCl (pH 8.0) and twice with RIPA lysis buffer for each sample. All washes were performed at 4°C. The proteins were eluted off of the beads by boiling the samples in 2x LDS sample buffer (Invitrogen, NP0007). The eluted fraction was run on a gel (Invitrogen, NP0341) for a 10 minutes. The resulting gel plug was stained (Invitrogen, 46-5034) and excised and sent to the Yale Keck facility for mass spectrometry analysis.

Mass spectrometry

MS was performed at Yale Mass Spectrometry & Proteomics Resource of the W.M. Keck Foundation Biotechnology Resource Laboratory. Samples were analyzed in biological triplicates. The data were normalized to internal controls and total spectral counts. For differential analysis between the two groups 10E-04 to was added to all values, the data was log2-transformed, and an unpaired Student t-test was performed. Differentially abundant proteins were considered those with an absolute fold change > 1.5 and $p < 0.05$.

FLASH-PAINT Imaging

Cells were fixed with 4% PFA (Electron Microscopy Services, 15710-S) for 30 min. After three washes in 1xPBS for five minutes each, cells were blocked and permeabilized with 3% BSA and 0.25% Triton X-100 at room temperature for 1 h. Next, cells were incubated with the anti-ARFGAP1 antibody, anti- Sec31A antibody, and the GFP-Nanobody in 3% BSA and 0.1% Triton X-100 at 4 °C overnight. Additionally, all other primary antibodies were pre incubated with the corresponding nanobodies (Tables S1) at 4 °C overnight. The next day, after four washes (30 s, 60 s, 2× 5 min) cells were incubated with the nanobodies corresponding to ARFGAP1 antibody and Sec31A antibody for ~2 h at room temperature. Next, unlabeled excess secondary nanobodies (to block unlabeled epitopes) were added to pre-incubation antibody-nanobody mixes at room temperature for 5 min. Next, the cells were incubated with the pooled antibody-nanobody mix for ~2.5 h at room temperature. After four washes (30 s, 60 s, 2× 5 min), the sample was post-fixed with 3% PFA and 0.1% GA for 10 min. Finally, samples were washed three times with 1× PBS for 5 min each before adding the imaging solution.

The imaging solution consisted of 1x PBS and 500 mM NaCl and was supplemented with 1× Trolox, (100× Trolox: 100 mg Trolox, 430 µL 100 % Methanol, 345 µL 1M NaOH in 3.2 mL H_2O), 1× PCA (40× PCA: 154 mg PCA, 10 mL water and NaOH were mixed and pH was adjusted 9.0), and 1× PCD (100× PCD: 9.3 mg PCD, 13.3 mL of buffer (100 mM Tris-HCl pH 8, 50 mM KCl, 1 mM EDTA, 50 % Glycerol)). All three stock buffers were frozen and stored at -20 °C.

Fluorescence imaging was carried out on an inverted Nikon Eclipse Ti2 microscope (Nikon Instruments) with the Perfect Focus System, attached to a Andor Dragonfly unit. The Dragonfly was used in the BTIRF mode, applying an objective-type TIRF configuration with an oil-immersion objective (Nikon Instruments, Apo SR TIRF 60×, NA 1.49, Oil). As excitation laser, a 561 nm (1W nominal) was used. The beam was coupled into a multimode fiber going through the Andor

Borealis unit reshaping the beam from a gaussian profile to a homogenous flat top. As dichroic mirror a CR-DFLY-DMQD-01 was used. Fluorescence light was spectrally filtered with an emission filter (TR-DFLY-F600-050) and imaged on a scientific complementary metal oxide semiconductor (sCMOS) camera (Sona 4BV6X, Andor Technologies) without further magnification, resulting in an effective pixel size of 108 nm. The power at the objective lens was ~10 % of the power set at the laser.

Imaging was carried out using the corresponding Imager and Adapter (Table S2, S3, S5) in imaging buffer. 25,000 frames were acquired at 25 ms exposure time. The readout bandwidth was set to 540 MHz. Laser power (@561 nm) was set to 80 mW (measured before the back focal plane (BFP) of the objective), corresponding to ~1.8 kW/cm^2 at the sample plane. After imaging the sample was subsequently washed three times with 200 µL each with 1× PBS (on the microscope) followed by an incubation with the corresponding eraser (Table S4; at 20 nM) for ~ 5 min. This process was repeated iteratively for ten sequential rounds (Table S5).

DNA-PAINT data was reconstructed, postprocessed (drift correction and alignment of imaging rounds) and rendered with the Picasso package[43].

Focused ion beam scanning electron microscopy and correlative light electron microscopy

For focused ion beam scanning electron microscopy (FIBSEM) CLEM, ATG2 DKO HEK293 cells overexpressing GFP-ATG2A were plated on 35-mm MatTek dish (MatTek, P35G-1.5-14-CGRD). The cells were starved for two hours prior to pre-fixation in 4% PFA + 0.25% glutaraldehyde and three washes in 1x PBS. Regions of interest by fluorescence light microscopy were selected and their coordinates on the dish were identified using phase contrast. Cells were further fixed with 2.5% glutaraldehyde in 0.1 M sodium cacodylate buffer, postfixed in 2% OsO4 and 1.5% K4Fe(CN)6 (Sigma-Aldrich) in 0.1 M sodium cacodylate buffer, en bloc stained with 2% aqueous uranyl acetate, dehydrated, embedded in Embed 812, and polymerized at 60°C for 48 hrs. Cells of interest were relocated based on the pre-recorded coordinates. Epon block was glued onto the SEM sample mounting aluminum stub and platinum en bloc coating on the sample surface was carried out with the sputter coater (Ted Pella, Inc.). The cell of interest was relocated under SEM imaging based on pre-recorded coordinates and FIB-SEM imaged in a Crossbeam 550 FIB-SEM workstation operating under SmartSEM (Carl Zeiss Microscopy GmbH) and Atlas 5 engine (Fibics, Inc.). The imaging resolution was set at 7 nm/pixel in the X, Y axis with milling being performed at 7 nm/step along the Z axis to achieve an isotropic resolution of 7 nm/voxel. Images were aligned and exported with Atlas 5 (Fibics, Inc.), further processed and segmented with DragonFly Pro software (Object Research Systems [ORS], Inc.).

Lysis, gel electrophoresis, and immunoblotting

Cells were collected by scraping in PBS. The cells were centrifuged at 500 g for 3 min at 4°C, and lysed in lysis buffer (10 mM Tris pH 7.5, 150 mM NaCl, 0.5 mM EDTA, 0.5% NP-40) with EDTA-free protease inhibitor cocktail (Sigma-Aldrich, 11873580001) on ice for five minutes. Lysates were collected after centrifugation at 16,000 g for 10 min at 4°C. Total protein concentration was determined by a bradford assay (BioRad, 5000006). 50-100 µM DTT (American Bio, AB00490-00010) and 1xLDS (Invitrogen, NP0007) loading buffer were added to each sample, which were then electrophoresed on precast Bis-Tris gels (Thermo Fisher Scientific, NP0341BOX or NP0342BOX). Gels were subsequently transferred to Immobilon-FL PVDF membranes (Sigma-Aldrich, IPFL00010) at 30-35 V for 90 min.

The membranes were blocked with 5% BSA (Sigma-Aldrich, A9647) in PBS-T (PBS containing 0.1% Tween 20; Thermo Scientific, CAS 9005-64-5) for 1 h at room temperature and incubated with primary antibody (diluted 1:1,000 in PBS-T containing 5% BSA [Sigma-Aldrich, A9647] and 0.03% sodium azide (Sigma-Aldrich, S2002)) overnight at 4°C. Membranes were washed three

times in PBS-T before incubation with the secondary antibody which was diluted 1:5,000 in PBS-T containing 0.5% Omniblock (American Bio, AB10109-00100) for 1 h. Membranes were then washed three times in PBST and treated with SuperSignal West Femto substrate (Thermo Fisher Scientific, 34096) for 5 min before imaging with the Bio-Rad VersaDoc imaging system.

Immunoprecipitation

For immunoprecipitation experiments, 15 cm plates were seeded and transfected upon reaching 80-90% confluency. The next day, the cells were collected by scraping, washed 1x in PBS, and lysed as previously described. Following quantification of protein levels by a Bradford assay, equal amounts of protein were added to pre-washed GFP-Trap beads (Proteintech, gtma-20). The volume was increased to 500 uL and the bead/lysate slurry was incubated at 4°C for two hours while rotating. The beads were pelleted using a magnetic rack and washed five times in lysis buffer (10 mM Tris pH 7.5, 150 mM NaCl, 0.5 mM EDTA, 0.5% NP-40) with EDTA-free protease inhibitor. The target proteins were eluted by boiling the beads for 10 min in 2x LDS loading buffer.

Densitometry and quantification

Densitometry quantifications of immunoblots and in-gel fluorescence images were performed using ImageJ software. For LC3B and P62 clearance analysis (Fig. S1 A-C), the band intensity of LC3B or P62 for each condition was normalized against the GAPDH intensity of that lane. To normalize each replicate, each value was divided by the mean value of the entire replicate. This normalization technique was also employed in the co-immunoprecipitation experiments. Statistical significance was determined by two-way ANOVA followed by a Tukey multiple comparison test to compare cell types. To quantify the co-immunoprecipitation reactions, the intensity of the 3xFLAG-ATG2A IP band was ratioed against the intensity of its corresponding input band. Following normalization, statistical significance was determined by a one (Fig. S3 A-D) or two-way (Fig. 2E-F) ANOVA followed by a Dunnett multiple comparison test to comparing each sample to the control lane. For the HaloTag flux assay (Fig. 2A, 2B, 3A, 3B), the Halotag flux rate was calculated as the ratio of the free Halotag band divided by the unprocessed Halotag band. Statistical significance was determined by a one (Fig. 2 A and B) or two-way (Fig 3 A and B) ANOVA followed by a Dunnett multiple comparison test to comparing each sample to the control lane. For one way ANOVA tests, data distributions were assumed to be normal. For two way ANOVA tests, the Geisser-Greenhouse correction was used as equal variability was not assumed. All data are $n = 3$ or greater and represent biological replicates. All data were plotted with mean ± SD, and all significance values were considering adjusted P value based on grouped analyses in Prism 9 (GraphPad). Asterisks indicate significance: *, $P < 0.05$; **, $P < 0.01$; ***, $P < 0.001$; ****, $P < 0.0001$. All blots were adjusted in contrast for better visualization of the bands in the figures.

LC3B flux analysis

WT, ATG2 DKO and ATG2 DKO + APEX2-GFP-ATG2A HEK293 cells were cultured in 6-well plates to 70-90% confluence. At the beginning of the assay, the media was replaced with fresh DMEM, DMEM containing 100 nM bafilomycin A1, or EBSS containing 100 nM bafilomycin A1. After a 2 hour incubation, cells were harvested by scraping, washed with 1x PBS, and lysed. 20 µg of protein from each sample were analyzed by SDS-PAGE and immunoblotting for ATG2A, P62, GAPDH, and LC3B.

HaloTag flux assay

HEK293 WT stably expressing either HaloTag7-mGFP or HaloTag7-mGFP-LC3B were cultured in 6-well plates to 60-70% confluence prior to transfection with either Sar1b/Sar1bH79G-mOrange2 for one day (Fig. 3A) or siRNA for two days (Fig. 2A). Sar1b transfection was

performed using Lipofectamine 3000 (Thermofisher Scientific, L3000015) according to the manufacturer's protocol. SiRNA transfection was performed using Dharmafect 1 (Horizon Discovery, T-2001-01) according to the manufacturer's protocol. The cells were incubated with 100 nm TMR-conjugated HaloTag ligand (Promega, G8251) for 30 min. Following two washes with 1xPBS, the cells were starved in EBSS for four hours. The cells were then collected and lysed. Following SDS-PAGE separation, in gel fluorescence was immediately measured with a ChemiDoc MP Imaging System (BioRad). Images were taken at 30 s and 100 s exposures. The gel was then transferred and immunoblotted against mCherry and GAPDH (Fig 3A) or FIP200, Rab1a, Rab1b, ARFGAP1, GAPDH, and LC3B (Fig 2A).

Immunofluorescence

Cells seeded on coverslips were fixed in 4% PFA (Electron Microscopy Sciences, 15710), washed three times with PBS, and permeabilized in PBS containing 0.1% Saponin (Sigma-Aldrich, 47036) and 3% BSA. Incubation with primary antibodies was done at 4C for 18-24 hrs and secondary antibodies at room temperature for 1 hr at indicated concentrations (see Reagents). After each antibody incubation, cells were washed three times in PBS containing 0.1% Saponin and 3% BSA. The coverslips were mounted on precleaned microscope slides with Fluoromont-G mounting reagent (Southern Biotech, 0100-01). Images were acquired on an inverted Zeiss LSM 880 laser scanning confocal microscope with AiryScan, using Zen acquisition software (Fig S1D) or a Nikon CSU-W1 SoRa 60x oil objective, using the Nikon Elements software (Fig. 1C, 3C-F, S3A, S3C, 4A, 4C, 4E, 4F). All images were processed using ImageJ software. Images are displayed either as maximum intensity projections or single confocal slices as stated in the figure legends.

To assess the enrichment factor of early secretory proteins around the ATG2 DKO compartment (Fig. 4D), the phagophore channel which was denoted by either LC3B or P62 was masked and duplicated. Following outlier removal, one masked image was dilated and the other eroded. Following an XOR function, the resulting signal formed a ring around the ATG2 DKO compartment and the early secretory protein channel(s) were measured using this ROI. Separately, the early secretory protein channel was masked using a manual threshold and measured. The enrichment factor was calculated as $(Mean_{compartment}-Min_{cell})/(Mean_{cell}-Min_{cell})$. Three biological replicates were combined and statistically assessed using a one-way ANOVA followed by a Dunnett multiple comparison test. All data were plotted with mean ± SD, and all significance values were considering adjusted P value based on grouped analyses in Prism 9 (GraphPad). Asterisks indicate significance: *, $P < 0.05$; **, $P < 0.01$; ***, $P < 0.001$; ****, $P < 0.0001$.

Live cell imaging

Cells were plated on poly-d-lysine coated MatTek dishes (MatTek, P35GC-1.5-14-C). The following day the cells were transfected using Lipofectamine 3000 (Thermo Fisher Scientific, L3000015) according to the manufacturer's protocol for 18-24 hrs. The cells were starved in HBSS (Thermo Fisher Scientific, 14025092) for 2-4 h and imaged in the same solution at 37°C. All images were analyzed using ImageJ and are displayed as maximum intensity projections.

For phagophore quantification (Fig. 1 C and D), each channel was masked using a manual threshold and outliers were removed. The ATG2A and LC3B channels were merged using the AND function and quantified as the total number of phagophores. The phagophore channel was then merged using the AND function with the transfected gene and quantified as the number of positive phagophores. Three biological replicates were combined and the ratio of positive over total was plotted and statistically assessed using a one-way ANOVA followed by a Dunnett multiple comparison test. All data were plotted with mean ± SD, and all significance values were considering adjusted P value based on grouped analyses in Prism 9 (GraphPad). Asterisks indicate significance: *, $P < 0.05$; **, $P < 0.01$; ***, $P < 0.001$; ****, $P < 0.0001$.

Data Availability

The data, code, protocols, and key lab materials used and generated in this study are listed in a Key Resource Table alongside their persistent identifiers at Table S6.

Acknowledgments

This work was supported by grants from the National Institutes of Health (R01 GM100930 and R35 GM153482 to TJM; R01 GM151829 to JB; DA018343 to PDC), F31 AG079606 to DMF and F31 DK136246 to JLK. This research was also funded in part through Aligning Science Across Parkinson's (ASAP-025173 to TJM and PDC) through the Michael J. Fox Foundation for Parkinson's Research (MJFF) and the Howard Hughes Medical Institute (HHMI; PDC). FS acknowledges support from the Human Frontier Science Program (LT000056/2020-C). JB acknowledges support by the Wellcome Leap Foundation. Imaging was supported by the Yale Center for Cellular and Molecular Imaging (both the fluorescence and electron microscopy facilities). We also thank the MS & Proteomics Resource at Yale University for providing the necessary mass spectrometers and the accompany biotechnology tools funded in part by the Yale School of Medicine and by the Office of The Director, National Institutes of Health (S10OD02365101A1, S10OD019967, and S10OD018034). The funders had no role in study design, data collection and analysis, decision to publish, or preparation of the manuscript.

References

1. Melia, T.J., Lystad, A.H. & Simonsen, A. Autophagosome biogenesis: From membrane growth to closure. *J Cell Biol* **219** (2020).
2. Osawa, T. *et al.* Atg2 mediates direct lipid transfer between membranes for autophagosome formation. *Nat Struct Mol Biol* **26**, 281-288 (2019).
3. Valverde, D.P. *et al.* ATG2 transports lipids to promote autophagosome biogenesis. *J Cell Biol* **218**, 1787-1798 (2019).
4. Maeda, S., Otomo, C. & Otomo, T. The autophagic membrane tether ATG2A transfers lipids between membranes. *Elife* **8** (2019).
5. Osawa, T., Ishii, Y. & Noda, N.N. Human ATG2B possesses a lipid transfer activity which is accelerated by negatively charged lipids and WIPI4. *Genes Cells* **25**, 65-70 (2020).
6. Matoba, K. *et al.* Atg9 is a lipid scramblase that mediates autophagosomal membrane expansion. *Nat Struct Mol Biol* **27**, 1185-1193 (2020).
7. Maeda, S. *et al.* Structure, lipid scrambling activity and role in autophagosome formation of ATG9A. *Nat Struct Mol Biol* **27**, 1194-1201 (2020).
8. Ghanbarpour, A., Valverde, D.P., Melia, T.J. & Reinisch, K.M. A model for a partnership of lipid transfer proteins and scramblases in membrane expansion and organelle biogenesis. *Proceedings of the National Academy of Sciences* **118**, e2101562118 (2021).
9. Olivas, T.J. *et al.* ATG9 vesicles comprise the seed membrane of mammalian autophagosomes. *J Cell Biol* **222** (2023).
10. Sawa-Makarska, J. *et al.* Reconstitution of autophagosome nucleation defines Atg9 vesicles as seeds for membrane formation. *Science* **369** (2020).
11. Ishihara, N. *et al.* Autophagosome Requires Specific Early Sec Proteins for Its Formation and NSF/SNARE for Vacuolar Fusion. *Molecular Biology of the Cell* **12**, 3690-3702 (2001).
12. Hamasaki, M., Noda, T. & Ohsumi, Y. The Early Secretory Pathway Contributes to Autophagy in Yeast. *Cell Structure and Function* **28**, 49-54 (2003).

13. Suzuki, K., Akioka, M., Kondo-Kakuta, C., Yamamoto, H. & Ohsumi, Y. Fine mapping of autophagy-related proteins during autophagosome formation in Saccharomyces cerevisiae. *Journal of cell science* **126**, 2534-2544 (2013).
14. Tan, D. *et al.* The EM structure of the TRAPPIII complex leads to the identification of a requirement for COPII vesicles on the macroautophagy pathway. *Proceedings of the National Academy of Sciences* **110**, 19432-19437 (2013).
15. Graef, M., Friedman, J.R., Graham, C., Babu, M. & Nunnari, J. ER exit sites are physical and functional core autophagosome biogenesis components. *Mol Biol Cell* **24**, 2918-2931 (2013).
16. Shima, T., Kirisako, H. & Nakatogawa, H. COPII vesicles contribute to autophagosomal membranes. *The Journal of cell biology* **218**, 1503-1510 (2019).
17. Ge, L., Melville, D., Zhang, M. & Schekman, R. The ER–Golgi intermediate compartment is a key membrane source for the LC3 lipidation step of autophagosome biogenesis. *eLife* **2** (2013).
18. Ge, L., Zhang, M. & Schekman, R. Phosphatidylinositol 3-kinase and COPII generate LC3 lipidation vesicles from the ER-Golgi intermediate compartment. *eLife* **3** (2014).
19. Hayashi-Nishino, M. *et al.* A subdomain of the endoplasmic reticulum forms a cradle for autophagosome formation. *Nat Cell Biol* **11**, 1433-1437 (2009).
20. Li, S. *et al.* A new type of ERGIC-ERES membrane contact mediated by TMED9 and SEC12 is required for autophagosome biogenesis. *Cell Res* **32**, 119-138 (2022).
21. Kumar, S. *et al.* Mammalian hybrid pre-autophagosomal structure HyPAS generates autophagosomes. *Cell* **184**, 5950-+ (2021).
22. Bozic, M. *et al.* A conserved ATG2-GABARAP family interaction is critical for phagophore formation. *EMBO Rep* **21**, e48412 (2020).
23. Feng, X. *et al.* Local membrane source gathering by p62 body drives autophagosome formation. *Nat Commun* **14**, 7338 (2023).
24. Velikkakath, A.K., Nishimura, T., Oita, E., Ishihara, N. & Mizushima, N. Mammalian Atg2 proteins are essential for autophagosome formation and important for regulation of size and distribution of lipid droplets. *Mol Biol Cell* **23**, 896-909 (2012).
25. Gudmundsson, S.R. *et al.* Morphology of Phagophore Precursors by Correlative Light-Electron Microscopy. *Cells* **11** (2022).
26. Hung, V. *et al.* Spatially resolved proteomic mapping in living cells with the engineered peroxidase APEX2. *Nat Protoc* **11**, 456-475 (2016).
27. Schueder, F. *et al.* Unraveling cellular complexity with transient adapters in highly multiplexed super-resolution imaging. *Cell* **187**, 1769-1784 e1718 (2024).
28. Weigel, A.V. *et al.* ER-to-Golgi protein delivery through an interwoven, tubular network extending from ER. *Cell* **184**, 2412-2429.e2416 (2021).
29. Wong-Dilworth, L. *et al.* Nanoscale imaging reveals the mechanisms of ER-to-Golgi transport via a dynamic tubular-vesicular network. *bioRxiv*, 2023.2010.2027.563951 (2023).
30. Westrate, L.M., Hoyer, M.J., Nash, M.J. & Voeltz, G.K. Vesicular and uncoated Rab1-dependent cargo carriers facilitate ER to Golgi transport. *J Cell Sci* **133** (2020).
31. Hein, M.Y. *et al.* Global organelle profiling reveals subcellular localization and remodeling at proteome scale. *Cell* (2024).
32. Yim, W.W., Yamamoto, H. & Mizushima, N. A pulse-chasable reporter processing assay for mammalian autophagic flux with HaloTag. *Elife* **11** (2022).
33. Lynch-Day, M.A. *et al.* Trs85 directs a Ypt1 GEF, TRAPPIII, to the phagophore to promote autophagy. *Proceedings of the National Academy of Sciences of the United States of America* **107**, 7811-7816 (2010).
34. Wang, J. *et al.* Ypt1 recruits the Atg1 kinase to the preautophagosomal structure. *Proc Natl Acad Sci U S A* **110**, 9800-9805 (2013).
35. Carlos Martín Zoppino, F., Damián Militello, R., Slavin, I., Álvarez, C. & Colombo, M.I. Autophagosome Formation Depends on the Small GTPase Rab1 and Functional ER Exit Sites. *Traffic* **11**, 1246-1261 (2010).

36. Gyurkovska, V. *et al.* Dual function of Rab1A in secretion and autophagy: hypervariable domain dependence. *Life Sci Alliance* **6** (2023).
37. Kotani, T., Kirisako, H., Koizumi, M., Ohsumi, Y. & Nakatogawa, H. The Atg2-Atg18 complex tethers pre-autophagosomal membranes to the endoplasmic reticulum for autophagosome formation. *Proceedings of the National Academy of Sciences of the United States of America* **115**, 10363-10368 (2018).
38. Yao, W. *et al.* TOR-mediated Ypt1 phosphorylation regulates autophagy initiation complex assembly. *EMBO J* **42**, e112814 (2023).
39. Tremel, S. *et al.* Structural basis for VPS34 kinase activation by Rab1 and Rab5 on membranes. *Nat Commun* **12**, 1564 (2021).
40. Cook, A.S.I. *et al.* Structural pathway for PI3-kinase regulation by VPS15 in autophagy. *Science*, eadl3787 (2025).
41. Bieber, A. *et al.* (Cold Spring Harbor Laboratory, 2022).
42. Holzer, E., Martens, S. & Tulli, S. The Role of ATG9 Vesicles in Autophagosome Biogenesis. *J Mol Biol* **436**, 168489 (2024).
43. Schnitzbauer, J., Strauss, M.T., Schlichthaerle, T., Schueder, F. & Jungmann, R. Super-resolution microscopy with DNA-PAINT. *Nat Protoc* **12**, 1198-1228 (2017).

Figures and Tables

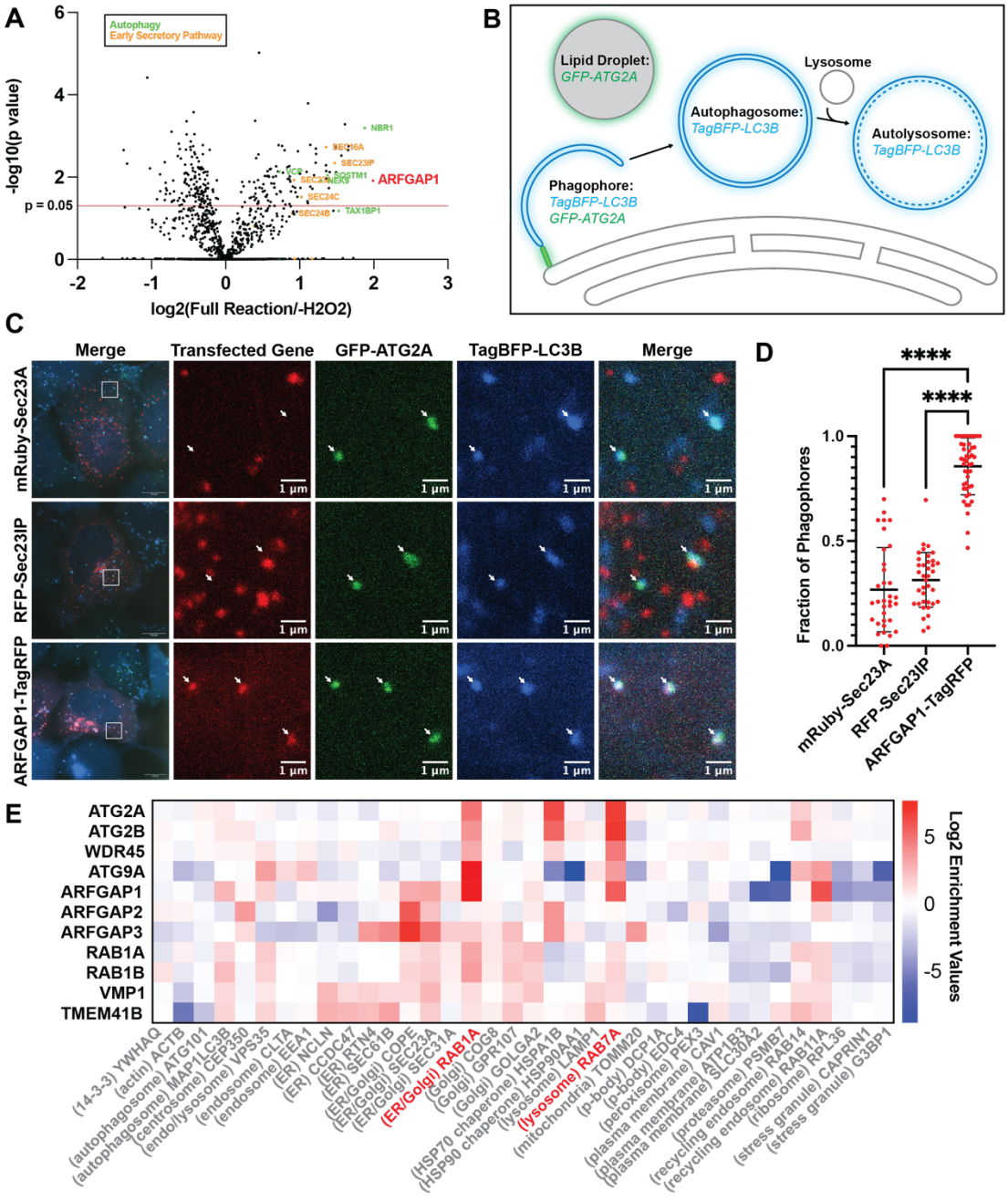

Figure 1. ATG2A is proximal to ARFGAP1 positive membranes. (A) Proximity labeling of HEK293 ATG2 DKO cells stably expressing APEX2-GFP-ATG2A was performed as previously described[26]. Three biological replicates were averaged and plotted as the log2 ratio between the full labeling reaction in complete media over cells that were not treated with hydrogen peroxide on the x axis, and -log10 of the p-value on the y axis. The red line demonstrates the p-value cutoff of 0.05. The proteomics revealed an enrichment of autophagy (labeled in green) and early secretory proteins (COPII/ER Exit Site proteins are labeled in orange, ARFGAP1 is labeled in red). **(B)**

Strategy to identify phagophores by live cell imaging. Phagophores are defined as sites where both GFP-ATG2A and TagBFP-LC3B co-localize. **(C-D)** Live cell imaging of ATG2 DKO cells stably expressing GFP-ATG2A and TagBFP-LC3B and transfected with mRuby-Sec23A or RFP-Sec23IP/p125a or ARFGAP1-TagRFP. The cells were starved for 2-4 hours prior to imaging. The fraction of phagophores (white arrows) that colocalized with the third fluorescent protein (transfected gene) was quantified and plotted in (D). Statistical significance was assessed by one way ANOVA. *, adjusted P value <0.05. **, adjusted P value <0.01. ***, adjusted P value <0.001. ****, adjusted P value <0.0001. Data from three biological replicates were pooled for each condition. Maximum intensity projections of confocal images. **(E)** Global organelle profiling data from https://organelles.sf.czbiohub.org[31]. Whole organelle profiles were established by pulling down endogenously tagged proteins and performing quantitative proteomics. The enrichment value for each protein were calculated by taking the difference in median log2 LFQ values between the replicates and the null distribution.

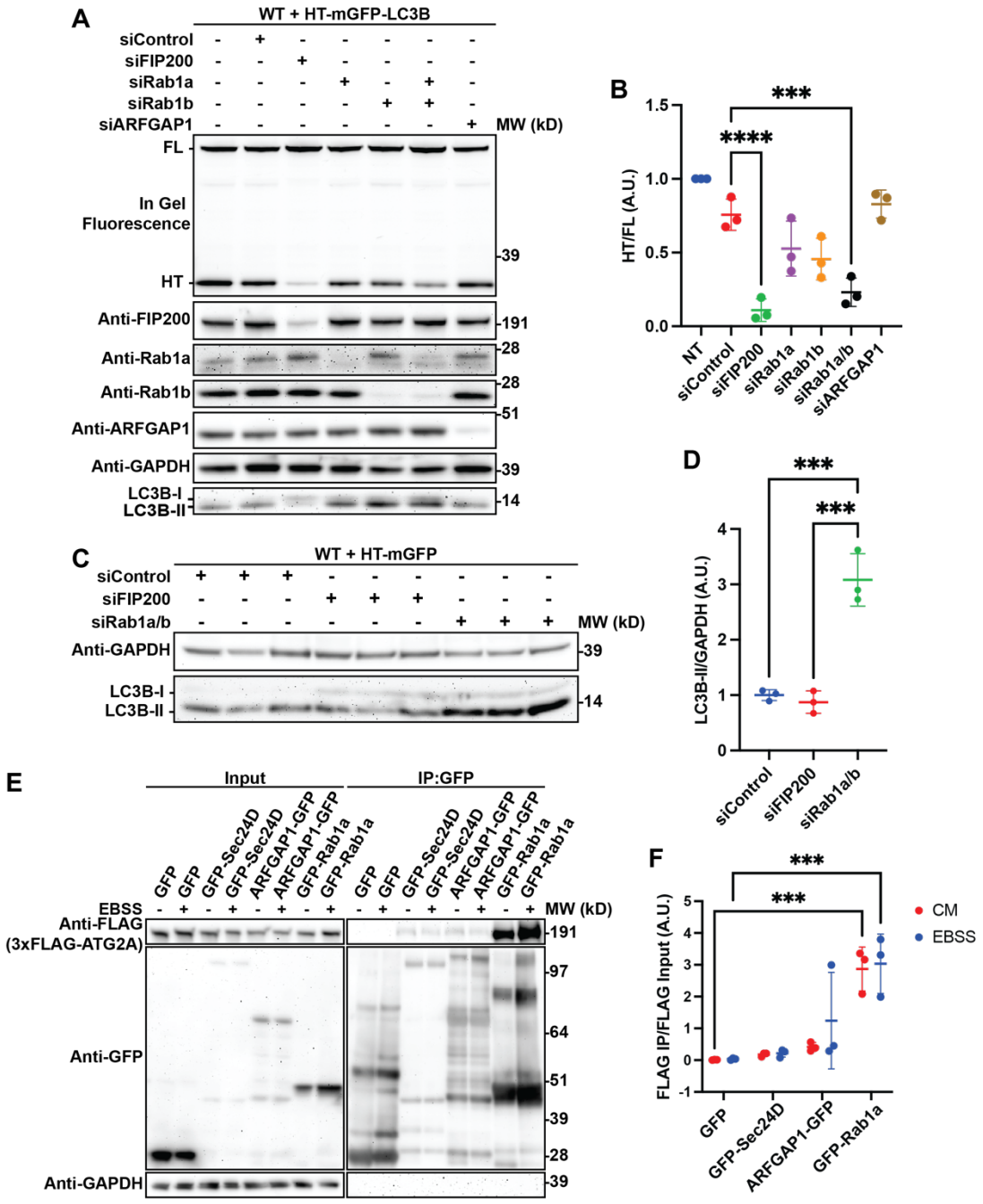

Figure 2. Autophagic flux depends upon Rab1 but not ARFGAP1. (A-B) In gel fluorescence image (top panel) and immunoblots demonstrating that siRNA KD of Rab1 inhibits autophagic flux. In gel fluorescence reveals HaloTag7s moeity bound to the TMR ligand. Indicated bands are full length (FL) HT-mGFP-LC3B protein and HaloTag7 after cleavage (HT) in the lysosome. The ratio between FL and HT demonstrates autophagic flux, quantified in (B). Statistical significance was assessed by one way ANOVA. *, adjusted P value <0.05. **, adjusted P value <0.01. ***, adjusted P value <0.001. ****, adjusted P value <0.0001. Data from three biological replicates were collected for each condition**. (C-D)** Immunoblot of lysates from three biological replicates demonstrating that siRNA KD of Rab1 results in an accumulation of LC3B-II. The band intensity

of LC3B-II was normalized against the intensity of GAPDH for each lane. To normalize each replicate, each individual value was divided by value of the non-transfected sample. Statistical significance was assessed by one way ANOVA. *, adjusted P value <0.05. **, adjusted P value <0.01. ***, adjusted P value <0.001. ****, adjusted P value <0.0001. **(E-F)** Immunoblot showing CoIP between GFP-Rab1a and 3xFLAG-ATG2A compared to the same reaction with other GFP-tagged early secretory proteins. The cells were incubated with either complete media or EBSS for four hours prior to harvesting. For the CoIP, ~3 mg of cell lysate was used per condition (slight deviations in total amount between replicates, but not between lanes). To quantify the results, the intensity of the 3xFLAG-ATG2A IP signal was ratioed against the input signal. To normalize each replicate, each individual value was divided by the average of the replicate. Statistical significance was assessed by two way ANOVA. *, adjusted P value <0.05. **, adjusted P value <0.01. ***, adjusted P value <0.001. ****, adjusted P value <0.0001. The media was not a significant source of variation (p = 0.3535).

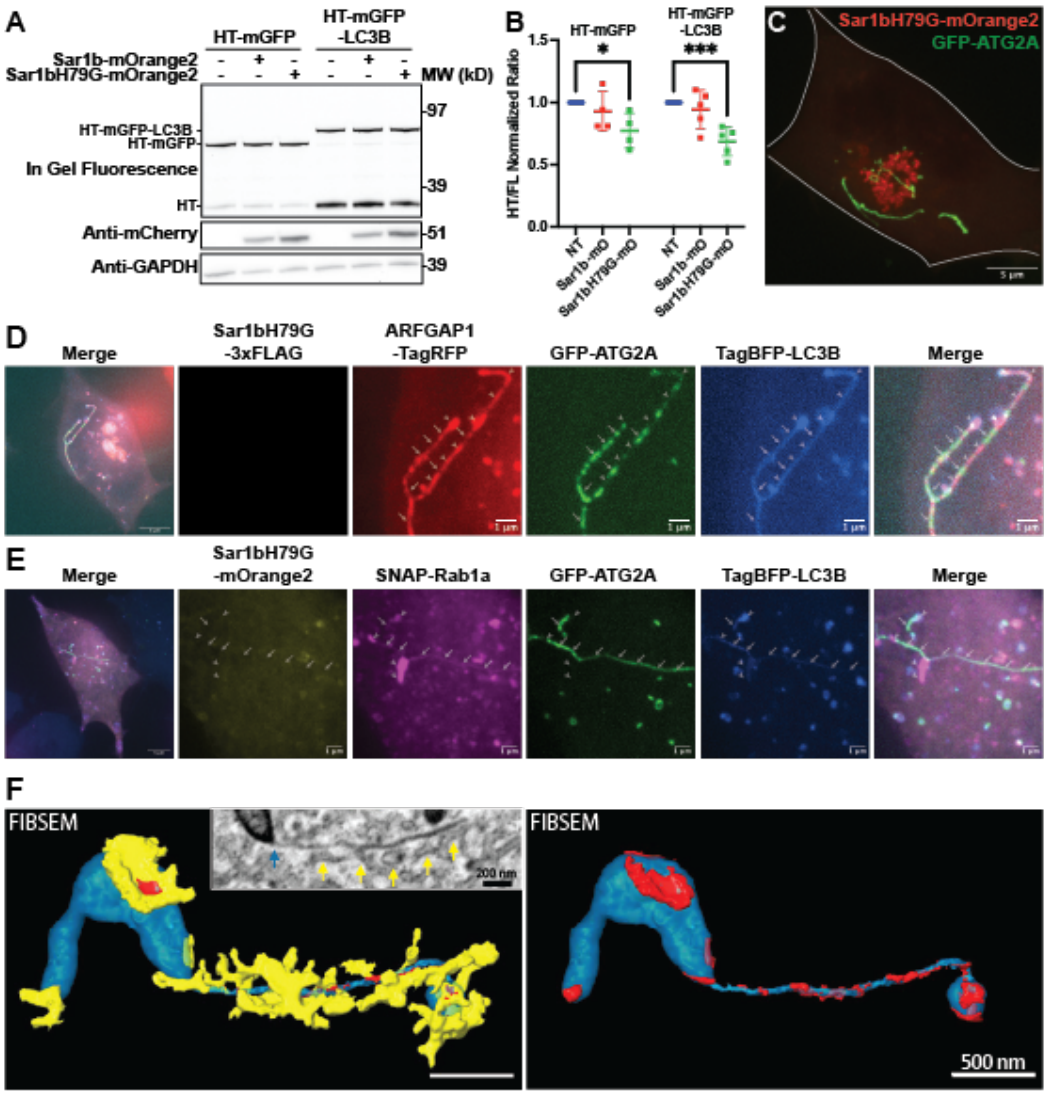

Figure 3. ATG2A, LC3B, ARFGAP1, and Rab1a localize to tubules following disruption of the early secretory pathway. (A-B) In gel fluorescence image (top panel) and immunoblots demonstrating that Sar1bH79G-mOrange2 (mO) overexpression negatively affects autophagic flux. The ratio between the FL and the free HT represents the autophagic flux in each condition (as in Fig. 2 A/B) and is plotted in (B). Statistical significance was assessed by two way ANOVA. *, adjusted P value <0.05. **, adjusted P value <0.01. ***, adjusted P value <0.001. ****, adjusted P value <0.0001. Data from four biological replicates were collected for each of the HT-mGFP conditions and five replicates were collected for each of the HT-mGFP-LC3B conditions. **(C)** Live cell imaging of ATG2 DKO cells stably expressing GFP-ATG2 that were transfected with Sar1bH79G-mOrange2 and starved for two hours. Note that GFP-ATG2A forms long tubules that do not colocalize with the Sar1bH79G-mOrange2 signal. Maximum intensity projection of a confocal image. Gray line was added to show cell outline. **(D-E)** Live cell imaging demonstrates the localization of ARFGAP1-TagRFP (D) and SNAP-Rab1a (E) on GFP-ATG2A/TagBFP-LC3B positive tubules following Sar1bH79G overexpression. Arrows denote thin GFP-ATG2A positive tubules whereas arrow heads denote thicker tubules that lack most GFP-ATG2A but contain high levels of LC3B, ARFGAP1, and Rab1a. Maximum intensity projections of confocal images. **(F)** CLEM-FIBSEM of cells prepared as in (C). GFP-ATG2A fluorescence corresponds to a thin

tubular membrane that is connected to a thicker tubule. The small inset in the left image shows a single SEM slice. The turquoise arrow is pointing to the tubule which is segmented and displayed in turquoise in the larger image, whereas the yellow arrows are pointing at adjacent ER tubules which are segmented and displayed in the larger image in yellow. At many points, these ER structures come into very close apposition with the tubule which is denoted in red. The ER structures are removed in the right image for better visualization of the ATG2A positive tubule. Note that only the thin section has corresponding GFP-ATG2A fluorescence.

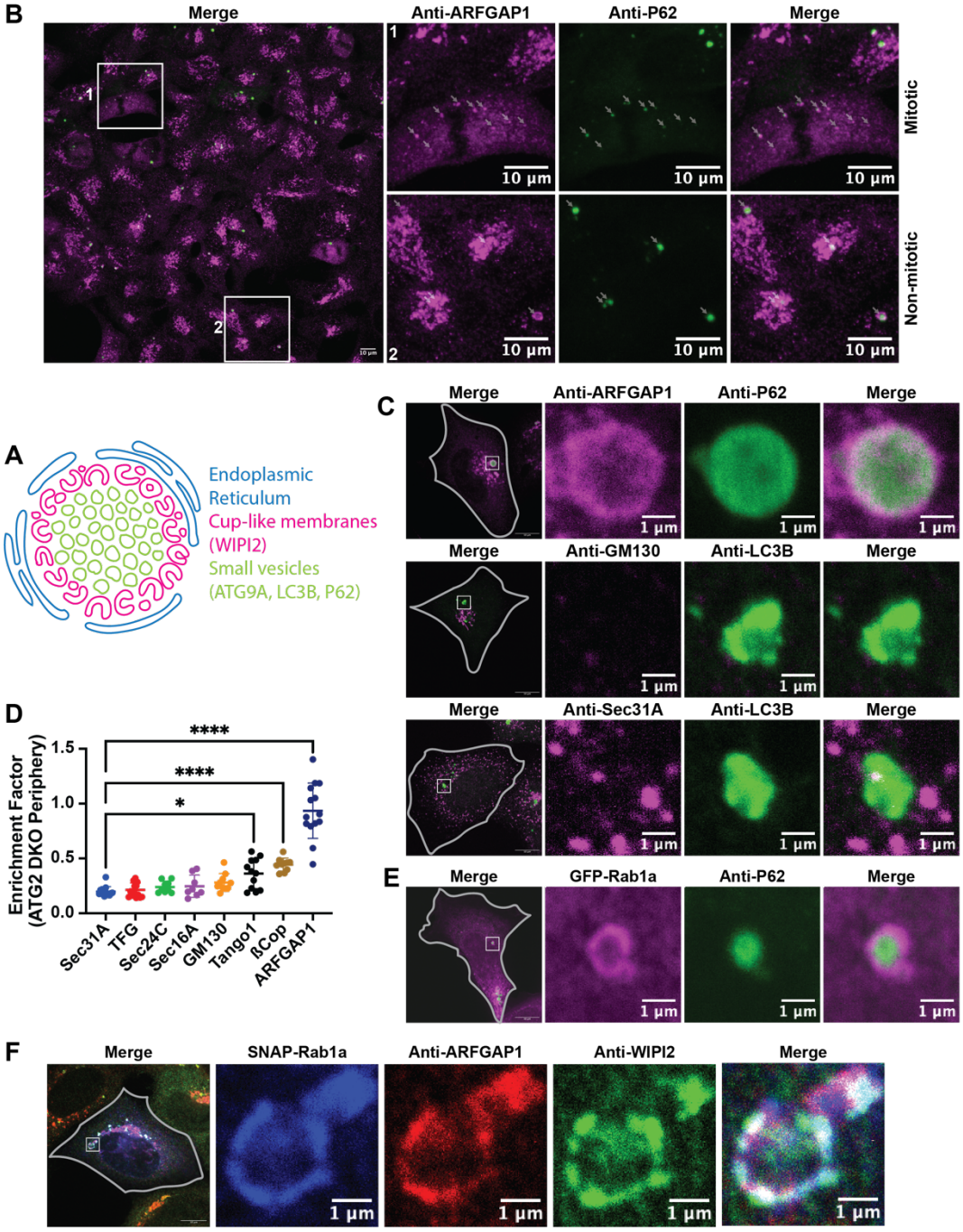

Figure 4. ATG2 deletion results in the accumulation of ARFGAP1 and Rab1a on autophagic membranes. (A) Schematic of the membranes that accumulate at the ATG2 DKO compartment based off the TEM images in Olivas et al[9]. The core of the compartment contains small vesicles that stain for ATG9A, LC3B, and P62. The periphery of the compartment is comprised of more complicated cup shaped membranes that stain for WIPI2. The entire compartment is enwrapped by ER tubules. **(B)** Immunofluorescence microscopy demonstrates that ARFGAP1 colocalizes with P62 in ATG2 DKO cells. Inset 1 highlights a cell undergoing mitosis, in which the colocalization of these two markers persists as denoted by the arrows. Inset 2 shows several

cells, a ring-like accumulation of ARFGAP1 around P62 is clearly visible, separate from the Golgi. Maximum intensity projection of a confocal image. **(C)** Immunofluorescence images demonstrating the distribution of early secretory membranes around the ATG2 DKO compartment which is marked by either P62 (mouse antibody) or LC3B (rabbit antibody). The images presented are single confocal slices of the center of the ATG2 DKO compartment. The gray lines show the cell periphery and the insets focus on the largest accumulation of P62 or LC3B in the cell. **(D)** Quantification of the images in (C) and in Sup Fig 4A. The enrichment factor is equal to the mean of the given protein at the periphery of the ATG2 DKO compartment compared to its mean throughout the cell. Statistical significance was assessed by one way ANOVA. *, adjusted P value <0.05. **, adjusted P value <0.01. ***, adjusted P value <0.001. ****, adjusted P value <0.0001. Data from three biological replicates were pooled together for each of the conditions. **(E-F)** Immunofluorescence images demonstrating the enrichment of overexpressed GFP-Rab1a (E) or SNAP-Rab1a (F) at the periphery of the ATG2 DKO compartment as determined by the presence of P62 (E) or WIPI2 (F). Presented as a single confocal slice. The gray lines show the periphery of the cell and the insets focus on ATG2 DKO compartments that are distal from the Golgi.

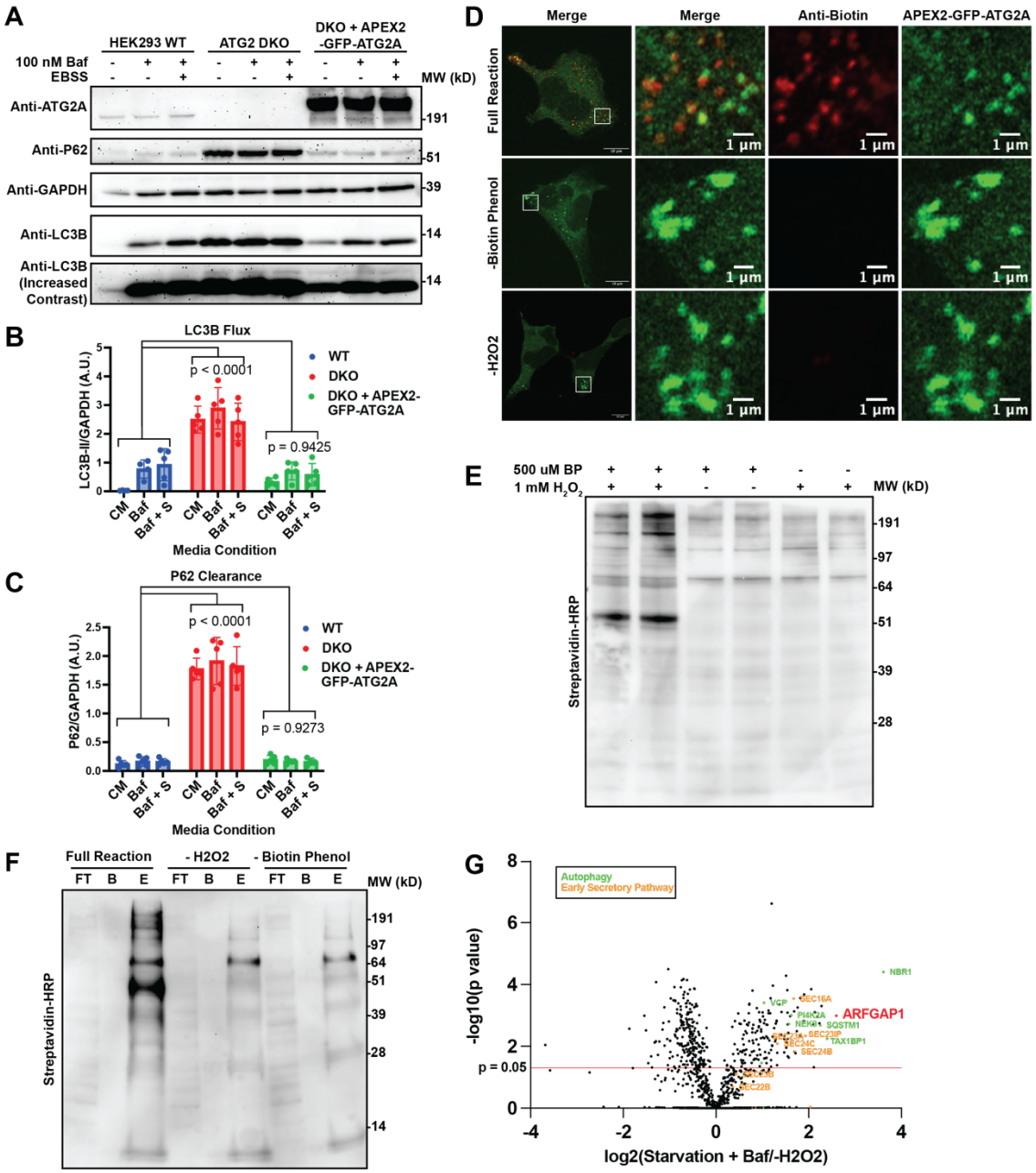

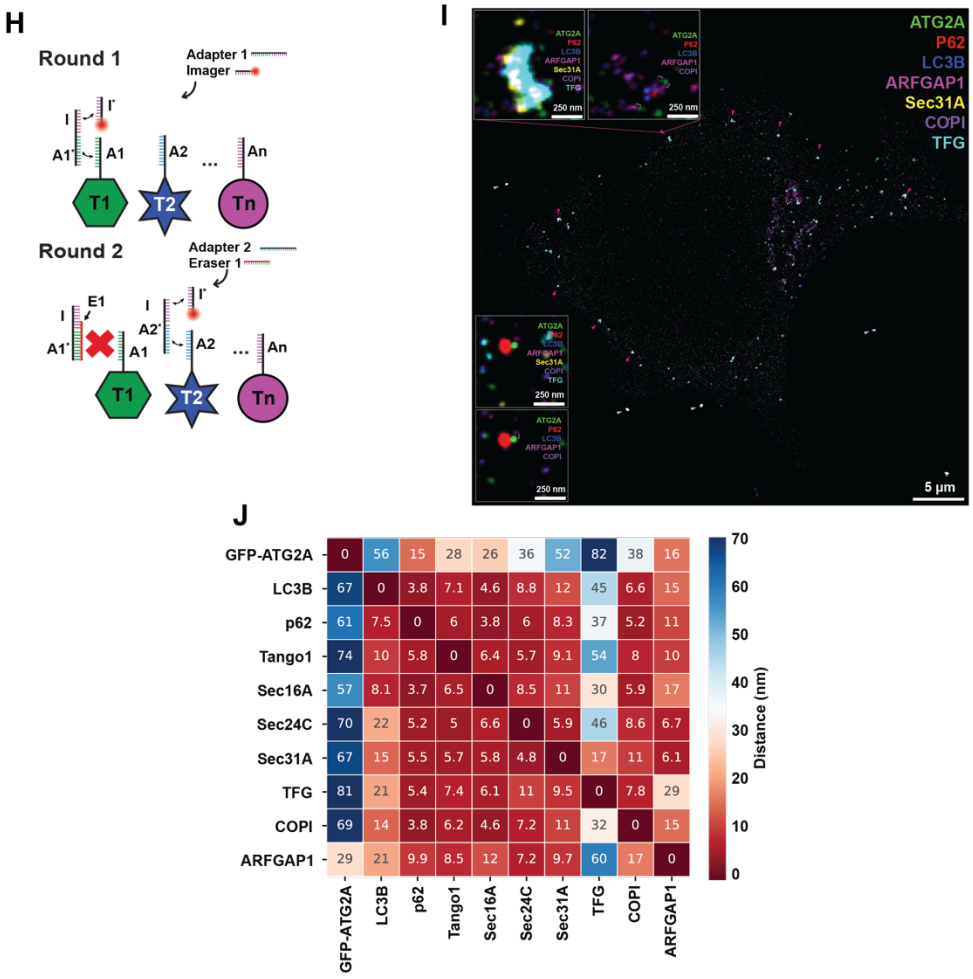

Supplemental Figure 1. ATG2A and ARFGAP1 colocalize during starvation. (A-C) Immunoblot showing the restoration of LC3B flux (B) and P62 clearance (C) in ATG2 DKO cells stably expressing APEX2-GFP-ATG2A. The restoration of a wild type phenotype indicates that the fusion protein is both localizing and functioning properly. The band intensity of LC3B (B) and P62 (C) were normalized against the intensity of GAPDH for each lane. To normalize each replicate, each individual value was divided by the average of the replicate. Statistical significance was assessed by two way ANOVA. Data from five biological replicates were collected for each condition, save for the WT + Baf and WT + Baf + EBSS, which each had four replicates. **(D-F)** Single slice confocal immunofluorescence images (D) and immunoblots (E-F) demonstrating that the addition of biotin phenol and hydrogen peroxide to ATG2 DKO cells stably expressing APEX2-GFP-ATG2A results in the biotinylation of proteins proximal to ATG2A. The omittance of either biotin phenol or hydrogen peroxide resulted in the loss of the anti-biotin signal, save for endogenously biotinylated proteins. The immunoblot in (F) demonstrates that the biotinylated proteins can be enriched on streptavidin beads. **(G)** Proximity labeling of HEK293 ATG2 DKO cells stably expressing APEX2-GFP-ATG2A was performed as described in Fig. 1A. **(H-J)** FLASH-PAINT analysis confirming the proximity of ATG2A to ARFGAP1. ATG2 DKO cells stably expressing GFP-ATG2A were labeled with all of the antibodies listed in (J), which in turn were preincubated with secondary antibodies with unique DNA sequences as depicted in (H). Each target (T1, T2… Tn) was visualized sequentially by adding an adaptor DNA strand that matched the target sequence (A1, A2… An) and an additional sequence to recruit the imager DNA strand (H). To remove the imager strand from each sequential target, a unique eraser strand was added

that recognized the entirety of the adaptor sequence (e.g. A1) and part of the imager sequence, resulting in the total sequestration of the adaptor DNA strand. The subsequent adaptor sequence was then added to visualize the next target protein. Seven of the ten visualized proteins are depicted in (I), which highlights the proximity of ATG2A and ARFGAP1 at autophagic and early secretory membranes. The heatmap presented in (J) shows the median distance within 200 nm between all visualized proteins. (I); pink arrow heads = ERES. white arrow heads = exogenous beads used as a fiduciary marks in imaging. (I; insets), brackets indicate immediate proximity of ATG2 (green) and ARFGAP (maroon) as frequently observed in ERES.

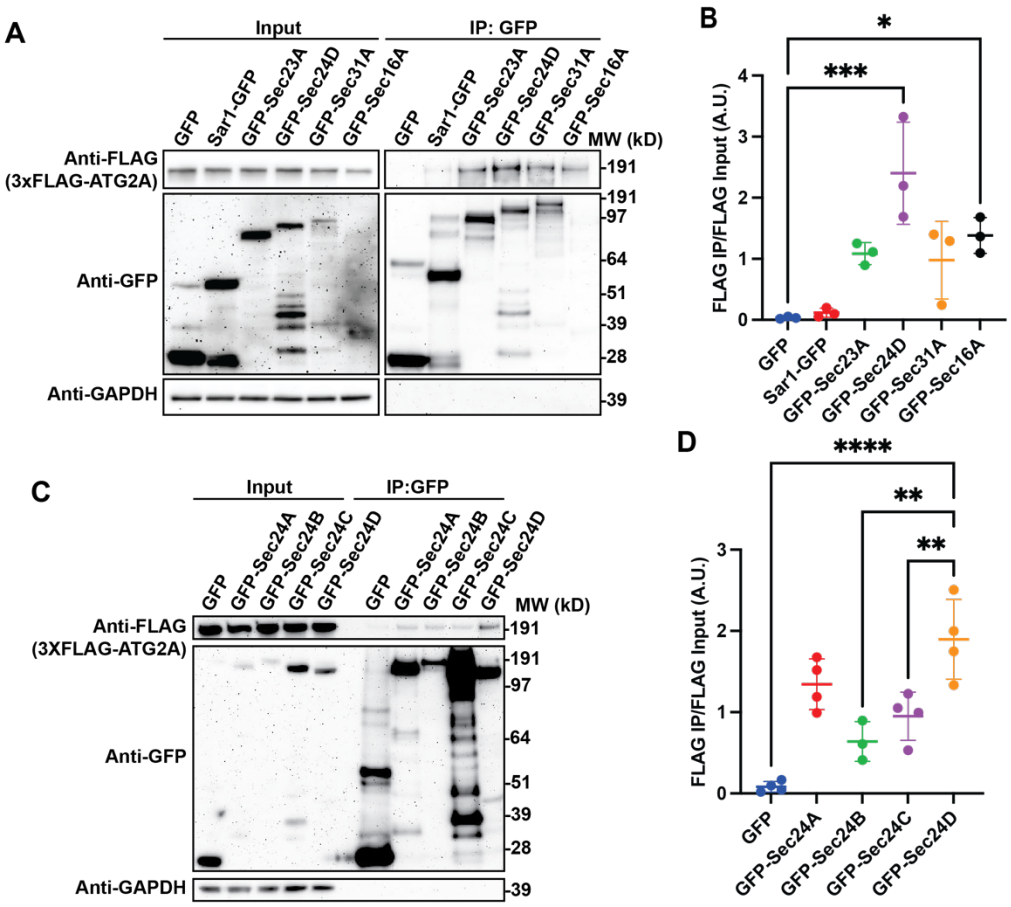

Supplemental Figure 2. ATG2A CoIPs weakly with ER Exit Site proteins. (A-D) Immunoblot showing the weak CoIP between 3xFLAG-ATG2A and various ER Exit Site proteins. For the CoIP, ~3 mg of cell lysate was used per condition (slight deviations in total amount between replicates, but not between lanes). Immunoblots quantified as in Fig. 2B. Statistical significance was assessed by one way ANOVA. *, adjusted P value <0.05. **, adjusted P value <0.01. ***, adjusted P value <0.001. ****, adjusted P value <0.0001.

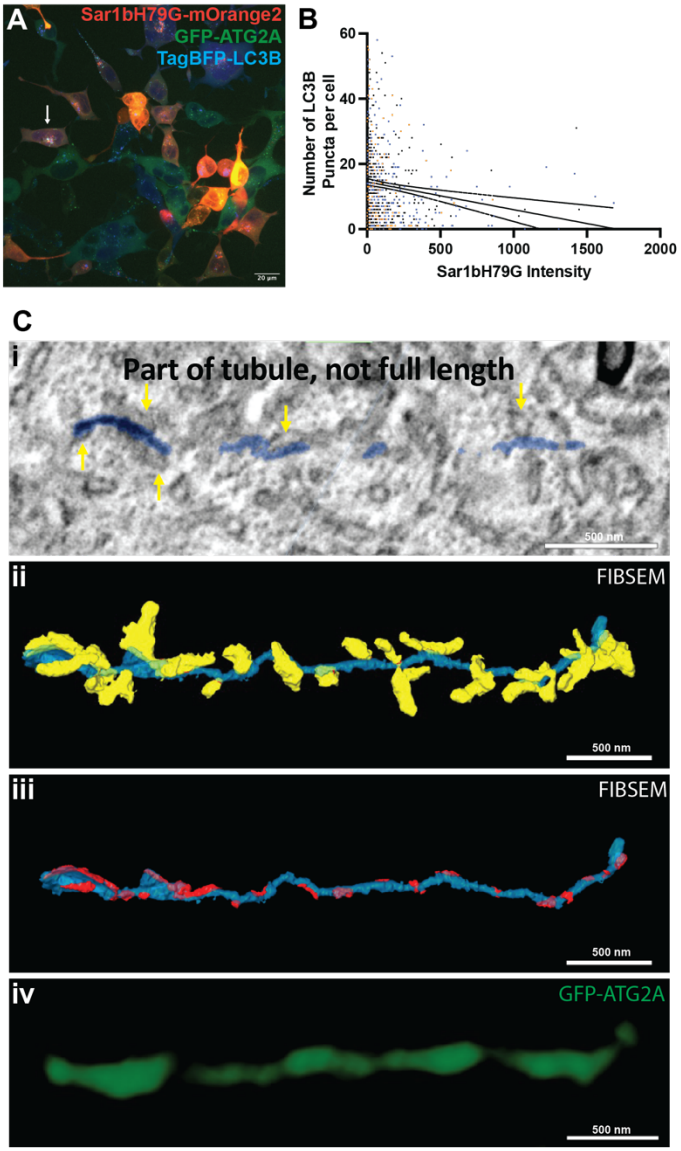

Supplemental Figure 3. Sar1bH79G overexpression hinders autophagy and leads to the formation of ATG2A positive membrane tubules. (A-B) Live cell imaging shows that Sar1bH79G overexpression negatively correlates with LC3B puncta number. ATG2 DKO cells stably expressing GFP-ATG2A and BFP-LC3B were transfected with Sar1bH79G-mOrange2 and starved for 2 hours. The number of transfected cells with GFP-ATG2A tubules (white arrow in A) was counted against the total number of transfected cells, resulting in a formation rate of 1.5±0.8%. ROIs were drawn over each transfected cell, and the resulting Sar1bH79G intensity was plotted against the number LC3B puncta in (B). A linear trendline was added in black with a 95% confidence interval. **(C)** CLEM-FIBSEM of cells prepared as in (Fig. 3C). GFP-ATG2A fluorescence corresponds to a thin tubular membrane. A single slice SEM slice is depicted in (i). Note that the segmented tubule comes in and out of the plane of this slice, so the tubule that is highlighted in turquoise is not complete. The yellow arrows are pointing at adjacent ER structures which are segmented and displayed in (ii) in yellow. At many points, these ER structures come into very close apposition with the tubule which is denoted in red. The ER structures are removed

in (iii) for better visualization of the tubule. The GFP-ATG2A fluorescence signal is depicted in (iv).

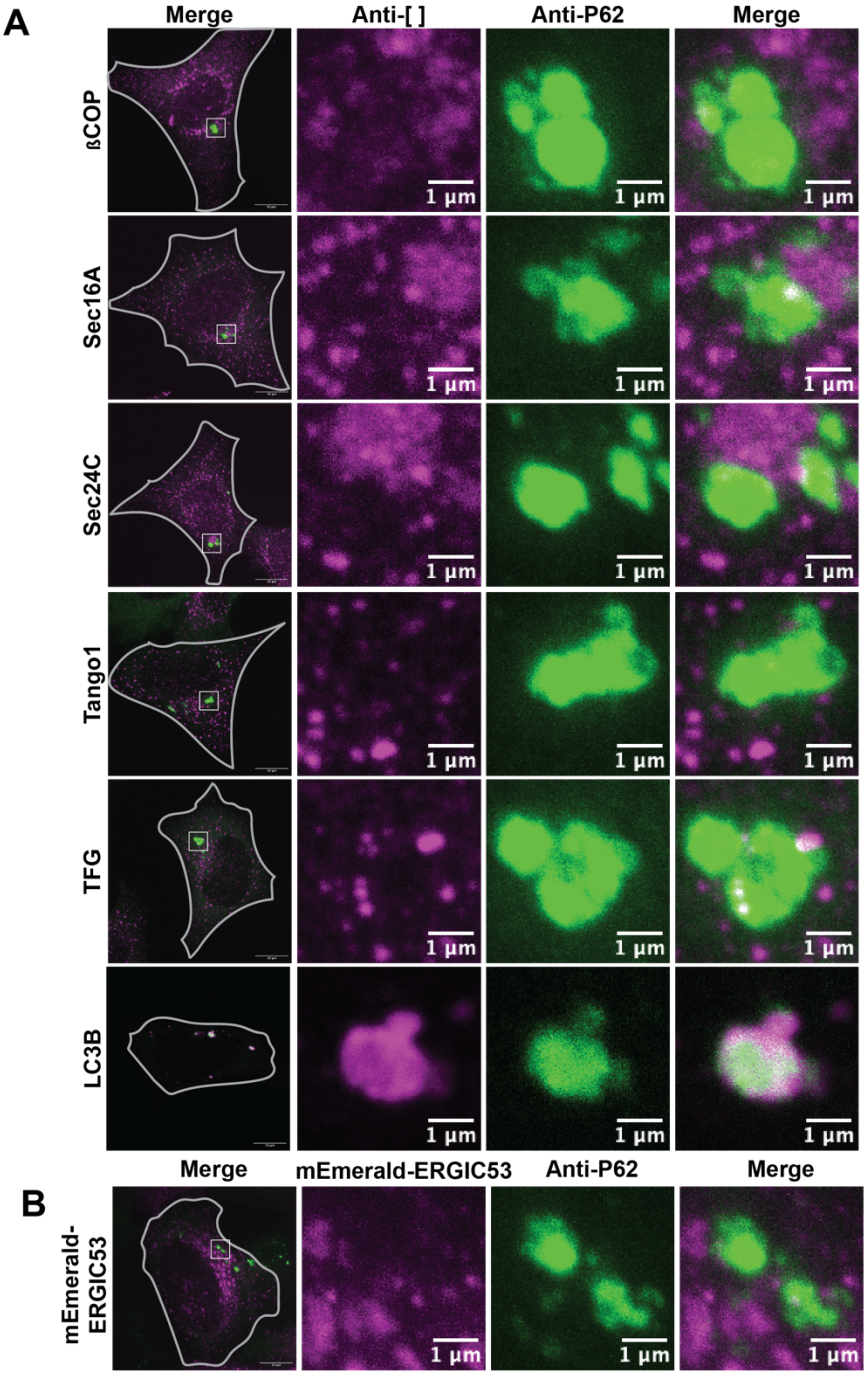

Supplemental Figure 4. Most early secretory markers are not enriched at the periphery of the ATG2 DKO compartment. (A-B) Immunofluorescence images demonstrating the distribution of endogenous (A) or overexpressed (B) early secretory membranes around the ATG2 DKO compartment which is marked by p62. The images presented are single confocal slices of the center of the ATG2 DKO compartment. The gray lines show the cell periphery, and the insets focus on the largest accumulation of p62 in the cell.

Table S1. Antibody Targets and Sequences for FLASH PAINT

Target	**Nanobody**	**Sequence (3' → 5')**
ATG2A-GFP	Anti-GFP-Nanobody-A3	NB - TT TCTTCATTAGCG
TFG	Anti-Rabbit-Nanobody-A15	NB - TT ATAGTGATTGGA
TANGO1	Anti-Rabbit-Nanobody- A39	NB - TT TTATGTTCTGCT
Sec24C	Anti-Rabbit-Nanobody-A8	NB - TT ATGTTAATGGGT
Sec16A	Anti-Rabbit-Nanobody-A38	NB - TT ATTTAGTGTAGC
LC3B	Anti-Rabbit-Nanobody-A20	NB - TT ATATGATCTCCG
Sec31A	Anti-Mouse-Nanobody-A27	NB - TT AAAAAGTTCGAG
ARFGAP1	Anti-Rabbit-Nanobody-A10	NB – TT ATAATGGATGGG
COPI	Anti-Mouse-Nanobody-A25	NB – TT ATAATCATGCTC
P62	Anti-Mouse-Nanobody-A36	NB – TT ATAACAGAATCG

Table S2. Imager Sequence

Imager name	**Sequence**	**3'-mod**
R2-6nt	TGGTGG	Cy3B

Table S3. Adaptor Sequences

Adapter Name	**Sequence (3' → 5')**
A3-5xR2	ACCACCACCACCACCACCA AA CGCTAATGAA
A15-5xR2	ACCACCACCACCACCACCA AA TCCAATCACT
A39-5xR2	ACCACCACCACCACCACCA AA AGCAGAACAT
A8-5xR2	ACCACCACCACCACCACCA AA ACCCATTAAC
A38-5xR2	ACCACCACCACCACCACCA AA GCTACACTAA
A20-5xR2	ACCACCACCACCACCACCA AA CGGAGATCAT
A27-5xR2	ACCACCACCACCACCACCA AA CTCGAACTTT
A10-5xR2	ACCACCACCACCACCACCA AA CCCATCCATT
A25-5xR2	ACCACCACCACCACCACCA AA GAGCATGATT
A36-5xR2	ACCACCACCACCACCACCA AA CGATTCTGTT

Table S4. Eraser sequences

Eraser Name	**Sequence (3' → 5')**
E3-5xR2	TTCATTAGCG TT TGG
E15-5xR2	AGTGATTGGA TT TGG
E39-5xR2	ATGTTCTGCT TT TGG
E8-5xR2	GTTAATGGGT TT TGG
E38-5xR2	TTAGTGTAGC TT TGG
E20-5xR2	ATGATCTCCG TT TGG
E27-5xR2	AAAGTTCGAG TT TGG
E10-5xR2	AATGGATGGG TT TGG
E25-5xR2	AATCATGCTC TT TGG
E36-5xR2	AACAGAATCG TT TGG

Table S5. Order of sequential antibody labeling for FLASH-PAINT

# Round	Protein	Adapter – Concentration	Imager – Concentration
Round 1	ATG2A-GFP	A3-5xR2 – 20 nM	R2 – 500pM
Round 2	ARFGAP1	A10-5xR2 – 20 nM	R2 – 250 pM
Round 3	Sec31A	A27-5xR2 – 20 nM	R2 – 500 pM
Round 4	Sec24C	A8-5xR2 – 20 nM	R2 – 500 pM
Round 5	Tango1	A39-5xR2 – 20 nM	R2 – 500 pM
Round 6	TFG	A15-5xR2 – 20 nM	R2 – 500 pM
Round 7	COPI	A25-5xR2 – 20 nM	R2 – 500 pM
Round 8	LC3B	A20-5xR2 – 20 nM	R2 – 500 pM
Round 9	P62	A36-5xR2 – 20 nM	R2 – 500 pM
Round 10	Sec16A	A38-5xR2 – 20 nM	R2 – 500 pM

Table S6. Key Resource Table

RESOURCE TYPE	RESOURCE NAME	SOURCE	IDENTIFIER	NEW/REUSE	ADDITIONAL INFORMATION
Antibody	ATG2A	Cell Signaling Technologies	AB_2732797	REUSE	
Antibody	P62	BD BioSciences	AB_398151	REUSE	
Antibody	GAPDH	Abcam	AB_307274	REUSE	
Antibody	LC3B	Cell Signaling Technologies	AB_2137707	REUSE	
Antibody	RB1CC1/FIP200	Thermo Fisher Scientific	AB_10666428	REUSE	
Antibody	Rab1a	Cell Signaling Technologies	AB_2665537	REUSE	
Antibody	Rab1b	Proteintech	AB_2237881	REUSE	
Antibody	ARFGAP1	Proteintech	AB_2058621	REUSE	
Antibody	FLAG	Sigma-Aldrich	AB_262044	REUSE	
Antibody	GFP	Cell Signaling Technologies	AB_1196615	REUSE	
Antibody	mCherry	Invitrogen	AB_2552323	REUSE	
Antibody	ECL anti-rabbit IgG horseradish peroxidase-linked	To be added later	To be added later	REUSE	
Antibody	ECL anti-mouse IgG horseradish peroxidase-linked	To be added later	To be added later	REUSE	
Antibody	Biotin	Rockland	AB_2611059	REUSE	
Antibody	GFP	Massive Photonics	To be added later	REUSE	
Antibody	Sec31A	BD BioSciences	AB_399717	REUSE	
Antibody	Sec24C	Cell Signaling Technologies	AB_2798565	REUSE	
Antibody	MIA3/Tango1	Sigma-Aldrich	AB_2682971	REUSE	
Antibody	TFG	Abcam	To be added later	REUSE	
Antibody	COPI/CMIA10	Rothman Lab	To be added later	REUSE	
Antibody	LC3B	MBL	AB_2274121	REUSE	
Antibody	Sec16A	Abcam	AB_1270588	REUSE	
Antibody	Sec24D	Cell Signaling Technologies	AB_2798574	REUSE	

Antibody	GM130	Proteintech	AB_2115327	REUSE	
Antibody	LMAN1/ERGIC 53	Abcam	AB_10973984	REUSE	
Antibody	Alexa Fluor 405 goat anti-mouse IgG	Invitrogen	AB_3251389	REUSE	
Antibody	Alexa Fluor 594 goat anti-rabbit IgG	Invitrogen	AB_3251387	REUSE	
Antibody	Alexa Fluor 647 goat anti-rabbit IgG	Invitrogen	AB_3251388	REUSE	
Antibody	Alexa Fluor 647 goat anti-mouse IgG	Invitrogen	AB_3668624	REUSE	
Recombinant DNA	pLVX Puro GFP-ATG2A	To be added later	To be added later	REUSE	
Recombinant DNA	pLVX Puro APEX2-GFP-ATG2A	This paper	To be added later	NEW	
Recombinant DNA	pcDNA3 APEX2-NES	To be added later	Addgene #49386	REUSE	
Recombinant DNA	pCMV 3xFLAG-ATG2A	To be added later	To be added later	REUSE	
Recombinant DNA	pLVX Neo TagBFP-LC3B	This paper	To be added later	NEW	
Recombinant DNA	pLVX-EGFP-IRES-Neo	To be added later	Addgene #128660	REUSE	
Recombinant DNA	pDESt47 Sar1-GFP	To be added later	Addgene #67409	REUSE	
Recombinant DNA	Sar1b-mOrange2	To be added later	Addgene #166899	REUSE	
Recombinant DNA	Sar1bH79G2-mOrange2	To be added later	Addgene #166900	REUSE	
Recombinant DNA	Sar1bH79G-3xFLAG	This paper	To be added later	NEW	
Recombinant DNA	mRuby-Sec23A	To be added later	Addgene 36158	REUSE	
Recombinant DNA	EGFP-Sec23A	To be added later	Addgene #66609	REUSE	
Recombinant DNA	pEGFP-Sec24A	This paper	To be added later	NEW	
Recombinant DNA	pEGFP-Sec24B	This paper	To be added later	NEW	
Recombinant DNA	EGFP-Sec24C	This paper	To be added later	NEW	
Recombinant DNA	pEYFP-Sec24C	To be added later	Addgene #66608	REUSE	
Recombinant DNA	pEGFP-Sec24D	To be added later	Addgene #32678	REUSE	

Recombinant DNA	GFP-Sec31A	To be added later	Addgene #42124	REUSE	
Recombinant DNA	GFP-Sec16A	To be added later	Addgene #36155	REUSE	
Recombinant DNA	ARFGAP1-TagRFP	To be added later	To be added later	NEW	
Recombinant DNA	ARFGAP1-GFP	Antonny Lab	To be added later	REUSE	
Recombinant DNA	pMRX IB HaloTag7-mGFP	To be added later	Addgene #184903	REUSE	
Recombinant DNA	pMRX No HaloTag7-mGFP-LC3B	To be added later	Addgene #184901	REUSE	
Recombinant DNA	pLVX puro GFP	This paper	To be added later	NEW	
Recombinant DNA	GFP-Rab1a	To be added later	To be added later	REUSE	
Recombinant DNA	SNAP-Rab1a	To be added later	To be added later	REUSE	
Oligonucleotide	APEX2_f	Keck Oligonucleotide Synthesis	N/A	GTATGAATTCATGgaaagtcttacccaactgtg	
Oligonucleotide	APEX2_r	Keck Oligonucleotide Synthesis	N/A	GGAAGTGAATTCggcatcagcaaacccaag	
Oligonucleotide	BamFLAGNotf	Keck Oligonucleotide Synthesis	N/A	CATGAGGATCCAGACTACAAAGACCATGACGGTGATTATAAAGATCATGACATCGATTACAAGGATGACGATGACAAGTAGGCGGCCGCACTAG	
Oligonucleotide	BamFLAGNotr	Keck Oligonucleotide Synthesis	N/A	CTAGTGCGGCCGCCTACTTGTCATCGTCATCCTTGTAATCGATGTCATGATCTTTATAATCACCGTCATGGTCTTTGTAGTCTGGATCCTCATG	
Oligonucleotide	24A_f	Keck Oligonucleotide Synthesis	N/A	GATCACTCGAGGTAGTGGAAGTGGAAGTATGTCCCAGCCGGGAATACC	

Oligonucleotide	24A_r	Keck Oligonucleotide Synthesis	N/A	GATCATTAATTAATCATTTATTCACTTGTTGCTGTATATGCAACAGGAATTCATAATATG	
Oligonucleotide	24B_f	Keck Oligonucleotide Synthesis	N/A	GATCACTCGAGGTAGTGGAAGTGGAAGTATGTCGGCCCCCGCCGGGTCCTCTCAC	
Oligonucleotide	24B_r	Keck Oligonucleotide Synthesis	N/A	GATCATTAATTAATCACTTACAAATCTGCTGCTGAACATGAAGCAAAAATTCATAGTAAG	
Oligonucleotide	pLVX-GFP_f	Keck Oligonucleotide Synthesis	N/A	gatctcgagctcaagcttcgaattcATGGTGAGCAAGGGCGAG	
Oligonucleotide	pLVX-GFP_r	Keck Oligonucleotide Synthesis	N/A	agaattatctagagtcgcgggatccTTACTTGTACAGCTCGTCCATG	
Oligonucleotide	Negative Control	Horizon Biosciences	D-001810-10-05	REUSE	siRNA
Oligonucleotide	FIP200	Horizon Biosciences	L-021117-00-0005	REUSE	siRNA
Oligonucleotide	Rab1a	Horizon Biosciences	L-0082383-00-0005	REUSE	siRNA
Oligonucleotide	Rab1b	Horizon Biosciences	L-008958-01-0005	REUSE	siRNA
Oligonucleotide	ARFGAP1	Horizon Biosciences	L-013321-02-005	REUSE	siRNA
Oligonucleotide	Anti-GFP label	Integrated DNA Technologies	N/A	TCTTCATTAGCG	
Oligonucleotide	Anti-TFG label	Integrated DNA Technologies	N/A	ATAGTGATTGGA	
Oligonucleotide	Anti-Tango1 label	Integrated DNA Technologies	N/A	TTATGTTCTGCT	
Oligonucleotide	Anti-Sec24C label	Integrated DNA Technologies	N/A	ATGTTAATGGGT	
Oligonucleotide	Anti-Sec16A label	Integrated DNA Technologies	N/A	ATTTAGTGTAGC	
Oligonucleotide	Anti-LC3B label	Integrated DNA Technologies	N/A	ATATGATCTCCG	
Oligonucleotide	Anti-Sec31A label	Integrated DNA Technologies	N/A	AAAAAGTTCGAG	

Oligonucleotide	Anti-ARFGAP1 label	Integrated DNA Technologies	N/A	ATAATGGATGGG	
Oligonucleotide	Anti-COPI/CMIA10 label	Integrated DNA Technologies	N/A	ATAATCATGCTC	
Oligonucleotide	Anti-P62 label	Integrated DNA Technologies	N/A	ATAACAGAATCG	
Oligonucleotide	Imager	Integrated DNA Technologies	N/A	TGGTGG	
Oligonucleotide	A3-5xR2	Integrated DNA Technologies	N/A	ACCACCACCACCACCACCAAA CGCTAATGAA	
Oligonucleotide	A15-5xR2	Integrated DNA Technologies	N/A	ACCACCACCACCACCACCAAA TCCAATCACT	
Oligonucleotide	A39-5xR2	Integrated DNA Technologies	N/A	ACCACCACCACCACCACCAAA AGCAGAACAT	
Oligonucleotide	A8-5xR2	Integrated DNA Technologies	N/A	ACCACCACCACCACCACCAAA ACCCATTAAC	
Oligonucleotide	A38-5xR2	Integrated DNA Technologies	N/A	ACCACCACCACCACCACCAAA GCTACACTAA	
Oligonucleotide	A20-5xR2	Integrated DNA Technologies	N/A	ACCACCACCACCACCACCAAA CGGAGATCAT	
Oligonucleotide	A27-5xR2	Integrated DNA Technologies	N/A	ACCACCACCACCACCACCAAA CTCGAACTTT	
Oligonucleotide	A10-5xR2	Integrated DNA Technologies	N/A	ACCACCACCACCACCACCAAA CCCATCCATT	
Oligonucleotide	A25-5xR2	Integrated DNA Technologies	N/A	ACCACCACCACCACCACCAAA GAGCATGATT	
Oligonucleotide	A36-5xR2	Integrated DNA Technologies	N/A	ACCACCACCACCACCACCAAA CGATTCTGTT	

Oligonucleotide	E3-5xR2	Integrated DNA Technologies	N/A	TTCATTAGCG TT TGG	
Oligonucleotide	E15-5xR2	Integrated DNA Technologies	N/A	AGTGATTGGA TT TGG	
Oligonucleotide	E39-5xR2	Integrated DNA Technologies	N/A	ATGTTCTGCT TT TGG	
Oligonucleotide	E8-5xR2	Integrated DNA Technologies	N/A	GTTAATGGGT TT TGG	
Oligonucleotide	E38-5xR2	Integrated DNA Technologies	N/A	TTAGTGTAGC TT TGG	
Oligonucleotide	E20-5xR2	Integrated DNA Technologies	N/A	ATGATCTCCG TT TGG	
Oligonucleotide	E27-5xR2	Integrated DNA Technologies	N/A	AAAGTTCGAG TT TGG	
Oligonucleotide	E10-5xR2	Integrated DNA Technologies	N/A	AATGGATGGG TT TGG	
Oligonucleotide	E25-5xR2	Integrated DNA Technologies	N/A	AATCATGCTC TT TGG	
Oligonucleotide	E36-5xR2	Integrated DNA Technologies	N/A	AACAGAATCG TT TGG	
Experimental model: Cell line	HEK293	WT Parental	ATCC CRL-1573	CVCL_0045	
Experimental model: Cell line	HEK293	ATG2 DKO	Valverde and Yu et al 2019	To be added later	
Experimental model: Cell line	HEK293	ATG2 DKO + APEX2-EGFP-ATG2A	This Study	To be added later	
Experimental model: Cell line	HEK293	ATG2 DKO + GFP-ATG2A	Valverde and Yu et al 2019	To be added later	
Experimental model: Cell line	HEK293	ATG2 DKO + GFP-ATG2A + TagBFP-LC3B	This Study	To be added later	
Experimental model: Cell line	HEK293	WT + HaloTag7-mGFP	This Study	To be added later	
Experimental model: Cell line	HEK293	WT + HaloTag7-mGFP-LC3B	This Study	To be added later	
Protocol	To be added later	protocols.io	To be added later	NEW	
Dataset	To be added later	Zenodo	To be added later	NEW	
Software/code	To be added later	Zenodo	To be added later	NEW	
Chemical, peptide, or	DMEM	Thermo Fisher Scientific	11965-092	REUSE	

recombinant protein					
Chemical, peptide, or recombinant protein	FBS	Thermo Fisher Scientific	16140-071	REUSE	
Chemical, peptide, or recombinant protein	PBS	Thermo Fisher Scientific	10010023	REUSE	
Chemical, peptide, or recombinant protein	Penicillin/Streptomicin (10,000 U/mL)	Thermo Fisher Scientific	15140122	REUSE	
Chemical, peptide, or recombinant protein	Blasticidin	Invivogen	Ant-bl-05	REUSE	
Chemical, peptide, or recombinant protein	Puromycin	Thermo Fisher Scientific	A11138-03	REUSE	
Chemical, peptide, or recombinant protein	Opti-Mem	Thermo Fisher Scientific	31985062	REUSE	
Chemical, peptide, or recombinant protein	Tris	American Bio	AB02000-05000	REUSE	
Chemical, peptide, or recombinant protein	NaCl	Sigma-Aldrich	24-May	REUSE	
Chemical, peptide, or recombinant protein	Hydrochloric Acid	J.T. Baker	9535	REUSE	
Chemical, peptide, or recombinant protein	SDS	American Bio	AB01920-00500	REUSE	
Chemical, peptide, or recombinant protein	EDTA	Sigma-Aldrich	3690	REUSE	
Chemical, peptide, or recombinant protein	Triton X-100	Sigma-Aldrich	X100	REUSE	

Chemical, peptide, or recombinant protein	Tween-20	Sigma-Aldrich	P7949	REUSE	
Chemical, peptide, or recombinant protein	Glycerol	American Bio	AB00751	REUSE	
Chemical, peptide, or recombinant protein	B-mercaptoethanol	Sigma-Aldrich	M3148	REUSE	
Chemical, peptide, or recombinant protein	HEPES (pH 7.4)	Thermo Fisher Scientific	15630-080	REUSE	
Chemical, peptide, or recombinant protein	DMSO	Sigma-Aldrich	D2650	REUSE	
Chemical, peptide, or recombinant protein	COmplete mini EDTA Free	Roche	1.1836E+10	REUSE	
Chemical, peptide, or recombinant protein	BSA	Sigma-Aldrich	A9647	REUSE	
Chemical, peptide, or recombinant protein	Non-Fat Dry Milk Omniblock	American Bio	AB10109-01000	REUSE	
Chemical, peptide, or recombinant protein	0.45 um Nitrocellulose Membrane	Thermo Fisher Scientific	1620115	REUSE	
Chemical, peptide, or recombinant protein	SuperSignal West Pico PLUS Chemiluminescence Substrate	Thermo Fisher Scientific	34580	REUSE	
Chemical, peptide, or recombinant protein	SuperSignal West Femto Maximum Sensitivity Substrate	Thermo Fisher Scientific	34095	REUSE	
Chemical, peptide, or	Methanol	Sigma-Aldrich	179337-4L-PB	REUSE	

recombinant protein					
Chemical, peptide, or recombinant protein	Ethanol	Decon Laboratories	2716	REUSE	
Chemical, peptide, or recombinant protein	Ampicillin	Sigma-Aldrich	A0166	REUSE	
Chemical, peptide, or recombinant protein	Paraformaldehyde	Electron Microscopy Sciences	19202	REUSE	
Chemical, peptide, or recombinant protein	Fisherbrandô Superfrostô Disposable Microscope Slides	Thermo Fisher Scientific	12-550-143	REUSE	
Chemical, peptide, or recombinant protein	Microscope Cover Slips (12 mm)	Carolina Biological Supply	633029	REUSE	
Chemical, peptide, or recombinant protein	Q5 High-Fidelity 2X Master Mix	NEB	M0492S	REUSE	
Chemical, peptide, or recombinant protein	HIFI DNA Assembly Master Mix	NEB	E2621L	REUSE	
Chemical, peptide, or recombinant protein	One-Shot STABL3	Invitrogen	C7373-03	REUSE	
Software/Code	Prism 10	Graphpad	SCR_002798	REUSE	
Software/Code	2.14.0/1.54f	FIJI	SCR_002285	REUSE	